UNIVERSITÀ DEGLI STUDI DI MILANO

DIP. DI BIOTECNOLOGIE MEDICHE E MEDICINA TRASLAZIONALE

Ph.D. PROGRAM
EXPERIMENTAL MEDICINE AND MEDICAL BIOTECHNOLOGIES

XXX Cohort

MED/03

IDENTIFICATION OF NOVEL MECHANISMS FOR NEUROLOGICAL CONDITIONS OVERLAPPING SMITH-MAGENIS SYNDROME

Tutor: Prof. Palma FINELLI
Supervisor: Prof. Antonia RATTI
PhD program Coordinator: Prof. Massimo Locati

Ph.D. thesis:
Dr. Maria SCIARRILLO
R10967

Academical Year 2016/2017

To MP, D, S, P and P

INDEX

ABSTRACT

Smith Magenis Syndrome (SMS, OMIM#182290) is a sporadic dominant disorder, with an estimated prevalence of 1:15000-25000 and results from *RAI1* gene haploinsufficiency due to either 17p11.2 deletion or *RAI1* mutation. SMS has a clinically recognizable phenotype characterized by distinct physical features, neurodevelopmental delay, cognitive impairment and behavioral problems which are reported in 75-100% of SMS cases, and include remarkable sleep disturbance (primarily due to circadian rhythms impairment), stereotypies, maladaptive, self-injurious behavior and sensory processing issues. SMS diagnosis is challenging due to the lack of a striking early childhood facial phenotype, maladaptive behavior that escalates with age, and overlapping syndromes that share with SMS most of the clinical signs and might switch to a differential diagnosis, i.e. 2q23.1 deletion syndrome (OMIM#156200) and Brachydactly Mental Retardation syndrome (BDMR, OMIM#600430).

Despite *RAI1* is recognized as the disease-causing gene, 50% of patients with a clinical suspicion of SMS do not have the classical genetic defects, thus it is likely that at genomic level other loci different from *RAI1*, if disrupted, eventually explain SMS similar phenotypes (SMS-like). Hence, even if several animal models support *RAI1* crucial contribution to brain development and plasticity, by interacting at chromatin promoter and enhancer regions, compelling evidences on its function, regulators, interactors, and targets are still missing.

In order to unveil the molecular basis of SMS-like syndrome and to clarify RAI1 molecular function, the main aim of this project will be a genetic and functional investigation of *RAI1* and candidate genes possibly implicated in SMS-like clinical manifestation.

A previously selected cohort of 40 SMS-like patients with a clinical suspicion of SMS but without the classical microdeletion at 17p11.2 or *RAI1* mutation was available in Medical Cytogenetics and Molecular Genetics Laboratory. High resolution array CGH screening of whole cohort was used to identify Copy Number Variants (CNVs) potentially containing dosage-sensitive genes eventually involved in neurological integrity maintenance, cognition and development, thus putatively implicated in SMS and “SMS-like” clinical condition. Among 40 SMS-like patients cohort the whole genome analysis pinpointed the attention on a CNV, specifically a 54 kb maternal deletion on Xq13.3 (chrX:74772380-74826319, hg19) in one male patient (SMS1). The Xq13.3 deletion does not involve any gene but contains highly conserved region, a predicted insulator and maps 29 kb far from 5’ end of the *ZDHHC15* (Zinc Finger DHHC domain-containing protein 15) gene which encodes for palmitoyl-transferase 15 ubiquitously expressed, but highly expressed in the brain. *ZDHHC15* was considered an interesting gene possibly implicated in patient phenotype onset due to its function and because was previously associated to a nonsyndromic X-linked intellectual disability. RT-qPCR and digital PCR analyses performed on SMS1 cDNA from peripheral blood revealed a significant downregulation of the *ZDHHC15* transcript, supporting that the CNV involving a predicted insulator element results in gene expression alteration by a position effect. Consistent with a possible involvement of *ZDHHC15* in SMS-like

phenotypes, subsequent Sanger sequencing of all male patients within the cohort was performed and identified a maternally inherited transversion, c.*182A>C, on *ZDHHC15* 3'UTR in a second male patient (SMS2). In order to clarify any transcriptional effect on *ZDHHC15* regulation caused by transversion, both relative RT-qPCR and digital PCR were carried out and allowed to show a slight but not significant *ZDHHC15* downregulation in SMS2 cDNA from peripheral blood. Since 3'UTR can be target of several miRNAs playing a role in mRNA regulation, was investigated if in SMS2 the c.*182A>C variant might have altered the normal target region of any miRNAs. Bioinformatic tools enable to select two miRNAs predicted to interact specifically with wild type *ZDHHC15* 3'UTR (miR-142-5p and miR-5590-3p) and three specifically with mutated *ZDHHC15* 3'UTR (miR-922; miR-191-5p and miR-4797-5p). Luciferase assay on HEK293T validated a specific and significant effect on wild type *ZDHHC15* 3'UTR sequence for miR-5590-3p and on mutated *ZDHHC15* 3'UTR sequence for miR-4797-3p, supporting the initial hypothesis of a possible transcriptional alterations due to A>C transversion.

The identification of two different alterations on *ZDHHC15* regulatory regions in two unrelated cases in such small cohort of SMS-like patients further supported the possible direct or indirect involvement of ZDHHC15 in RAI1 pathway.

To test *in vitro* whether a transient knockdown of *RAI1* and *ZDHHC15* would lead to change in expression of genes associated to the regulation of circadian rhythms we used silencing experiments on human BE(2)-M17 neuroblastoma cell line. Both *RAI1* and *ZDHHC15* silenced cells displayed significant deregulation of expression in up to half of the circadian genes. Moreover, nine out of main sixteen circadian gene proteins tested were predicted to be palmitoylated supporting an eventual role of ZDHHC15 in circadian rhythms control. *In silico* palmitoylation predictions and silencing experiments corroborate the idea of interconnection among RAI1, ZDHHC15 and circadian rhythms, but further analysis are needed to get a mechanistic insight.

In conclusion the combined genomic and functional approach used, highlight *ZDHHC15* as a promising candidate gene involved in SMS/SMS-like phenotypes.

INTRODUCTION

1.1_Smith Magenis Syndrome

1.1.1_Clinical overview

Smith Magenis Syndrome (SMS, OMIM#182290) is a sporadic dominant disorder, with an estimated prevalence of 1:15000-25000, described for the first time by Smith ACM et al. in 1986 (Smith et al 1986). SMS results mainly from haploinsufficiency of *RAI1* gene due to either 17p11.2 deletion or *RAI1* mutation, males and females are equally affected (Edelman et al 2007).

SMS has a clinically recognizable phenotype characterized by distinct physical features, neurodevelopmental delay, cognitive impairment and behavioural problems. SMS patients show peculiar craniofacial appearance, that usually progress with age, such as brachycephaly, midface hypoplasia, broad square-shaped face, and tented upper lip (Fig.1A-E) (Patil, Bartley 1984; Smith et al 1986; Smith et al 1991; Moncla et al 1991). Moreover they are characterized by skeletal features, including brachydactyly (Fig.1F-G), short stature and scoliosis, and otolaryngologic problems represented by hearing loss, chronic ear infections and hoarse deep voice (Greenberg et al 1996; Smith et al 2002) (Tab.1).

SMS individuals manifest a variable degree of intellectual disability along with a reduced sequential processing ability, short term memory and motor and speech delays. Behavioural features, reported in 75-100% of SMS cases, include remarkable sleep disturbance, stereotypies, maladaptive, self-injurious behavior and sensory processing issues. Despite these behavioural aspects represent pathognomonic signs of SMS disease generally are not recognized until age 20 months or older and evolve until adulthood (Dykens, Smith 1998; Smith et al 1998; Smith et al 1998; Sarimski 2004; Gropman et al 2006; Elsea, Girirajan 2008; Elsea, Girirajan 2011).

The lack of a striking infancy/early-childhood facial phenotype (Fig.1A-C) and behavioral issues make SMS diagnosis challenging and usually delayed to schooling age. Brachycephaly, broad forehead, upslanting palpebral fissures, short upturned nose, tented upper lip vermilion with mild micrognathia emerged in primary school ages (Fig.1A). At early school age deep-set eyes and midface retrusion crop up (Fig.1B-C) resulting in easily noticeable prognatism throughout adolescence (Fig.1D-E). Maladaptive behaviors escalate with age and are usually related to developmental delay, associated systemic disorders and sleep disturbance degree (Dykens, Smith 1998; Elsea, Girirajan 2008; Elsea, Girirajan 2011).

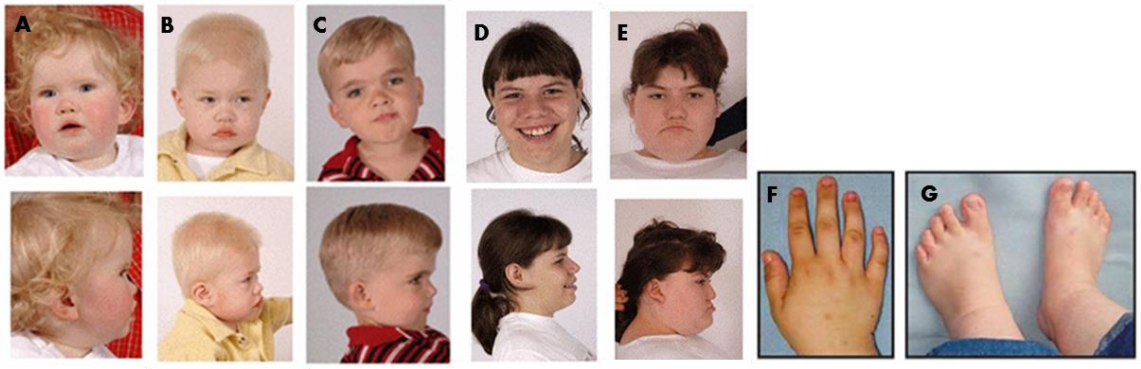

Fig. 1 (A) SMS Female with 17p11.2 deletion, age 9 months (B) SMS male with 17p11.2 deletion age 30 months, (C) SMS male with 17p11.2 deletion age 4 years; (D) SMS female with *RAI1* mutation, age 12 years; (E) SMS female with 17p11.2 deletion, age 15 years. (F-G) Hand and feet brachydactyly in a SMS patient (Elsea, Girirajan 2008; Williams et al 2010)

Tab.1 Clinical Features of Smith-Magenis Syndrome

Frequency	System	Finding
>75% of individuals	Craniofacial / Skeletal	Brachycephaly Midface retrusion Relative prognathism with age Broad, square-shaped face Everted, "tented"vermilion of the upper lip Deep-set, close-spaced eyes Short broad hands Dental anomalies (missing premolars; taurodontism)
	Otolaryngologic	Middle ear and laryngeal anomalies Hoarse, deep voice
	Neurobehavioral	Cognitive impairment/developmental delay Generalized complacency/lethargy (infancy) Infantile hypotonia Sleep disturbance Inverted circadian rhythm of melatonin Attention seeking Attention deficit (+/-hyperactivity) disorder Tantrums, behavioral outbursts Impulsivity Stereotypic behaviors Self-injurious behaviors Speech delay Hyporeflexia Signs of peripheral neuropathy Oral sensorimotor dysfunction (early childhood) Sensory processing issues
Common (50%-75% of individuals)		Hearing loss Short stature Scoliosis Mild ventriculomegaly of brain Hyperaccusis Tracheobronchial problems History of constipation Abnormal EEG without overt seizures Autism spectrum disorder (ASD)

Less common (25%-50% of individuals)		Cardiac defects Thyroid function abnormalities Seizures Immune function abnormalities (esp. low IgA)
Occasional (<25% of individuals)		Renal/urinary tract abnormalities Seizures Forearm abnormalities Cleft lip/palate Retinal detachment

Sleep disturbance represents a hallmark of this syndrome and polysomnography and actigraphy revealed a broad spectrum of sleep anomalies including/comprising difficulty falling asleep, decreased or increased REM, multiple awakening and overall reduction of total sleep timing (Boone et al 2011). Sleep disturbance results in >90% of cases from an inverted circadian rhythm of melatonin (Fig.2).

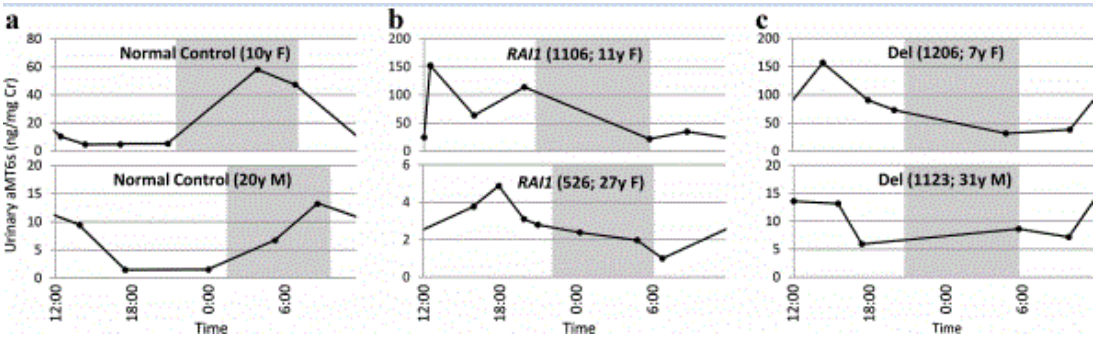

Fig.2-Melatonin rhythmicity is altered in *RAI1* mutated patients. Levels of urinary6-sulfatoxymelatonin (aMT6s), a surrogate for serum melatonin concentration, were determined over one day and normalized to urinary creatinine (Cr). A) In healthy individuals, the highest concentration of aMT6s is found in the first morning sample, reflecting the normal rise of serum melatonin during the night. B-C) This rhythmicity is inverted in *RAI1* mutated patients (B), similar to individuals with the SMS common deletion (C) Both children (top panel) and adult (bottom panel) are represented. Shaded areas indicate the period of darkness. *RAI1*, *RAI1* mutation; Del, common SMS deletion (Boone et al 2011).

A single study of SMS cases treated with oral β_1 antagonist acenbutolol triggers the suppression of daytime melatonin peaks and a subjective behavioural amelioration, while melatonin nocturnal plasma concentration did not improve (De Leersnyder et al 2001). Further studies showed that administration of acenbutolol to reduce daytime melatonin secretion in combination with an evening oral dose of control-release melatonin to restore nocturnal plasma melatonin levels, subjectively improving behaviour (De Leersnyder et al 2003).

Nevertheless two patients displaying a normal melatonin secretion were reported recently (Potocki et al 2000; Boudreau et al 2009), thus positing that an aberrant melatonin secretion pattern might be just one of the contributors to sleep disturbance phenotype in SMS patients.

1.1.2_SMS Overlapping Syndromes

Together with delayed onset of a clear craniofacial dysmorphism some overlapping syndromes make SMS diagnosis tricky. Indeed Smith-Magenis syndrome (SMS) might shift to differential diagnosis with some syndromes presenting developmental delay, infantile hypotonia, short stature, distinctive facies, and a behavioral phenotype including: Prader-Willi syndrome (PWS, OMIM#176270) Down syndrome, in the newborn period (OMIM#190685), Brachydactly Mental Retardation syndrome (BDMR, OMIM#600430), 2q23.1 deletion syndrome (OMIM#156200), and Kleefstra syndrome (OMIM#610253).

2q23.1 deletion syndrome shares with SMS the main clinical features concerning developmental delay, language impairment, behavioural problems and a variable degree of intellectual disability (Wagenstaller et at 2007; van Bon et al 2010; Williams et al 2010 a). In particular >90% of patients with 2q23.1 deletion have developmental, motor and speech delays along with autistic behaviour; hence sleep disturbance, short stature and craniofacial anomalies are observed in ~70% of cases (Mullegama et al 2015 a).

BDMR presents broad and heterogeneous clinical features depending on 2q37 deletion size (Wilson et al 1995; Giardino et al 2003; Villavicencio-Lorini et al 2013; Wheeler et al 2014; Jean-Marcais et al 2015). Due to BDMR stricking similarity to SMS patients were misdiagnosed (Williams et al 2010 a). BDMR syndrome resembles SMS facial dysmorphism, brachydactyly, mild to moderate intellectual disability, sleep disturbance, self-injurious behaviour by altered pain sensitivity and obesity.

A summary of both peculiar and common clinical traits are shown in Venn diagram below (Fig.3). Besides all two syndromes mentioned are also linked to SMS causing gene at molecular level (Williams et al 2010 b; Williams et al 2010 c; Mullegama et al 2015 a,b). The details will be described in the following paragraphs.

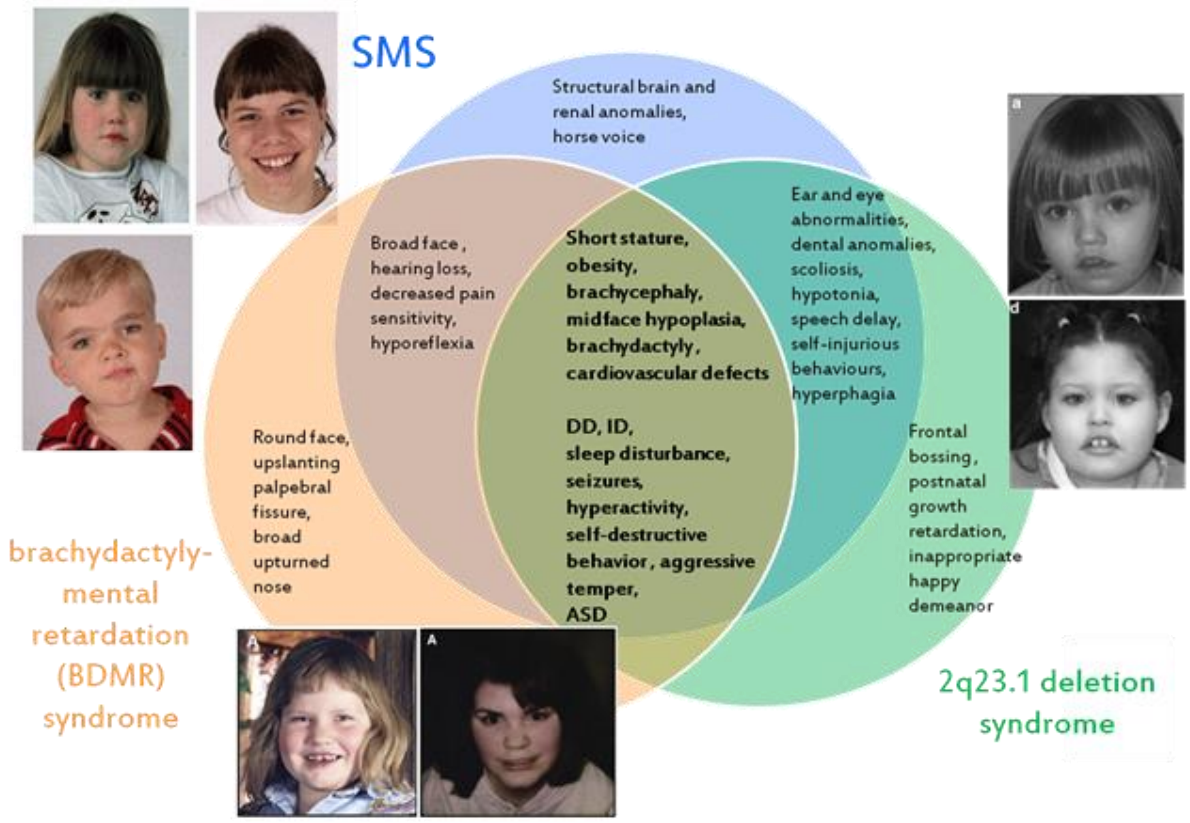

Fig. 3-Venn diagram showing overlapping and non-overlapping clinical features in SMS, 2q23.1 deletion and BDMR syndromes (patients pictures from Williams et al 2010 a).

Intriguingly Potocki-Lupski (PTLS, OMIM#610883), a developmental disorder caused by 17p11.2 reciprocal duplication (Brown et al 1996; Potocki et al 2000; Potocki et al 2007; Greco et al 2008), shares with SMS several clinical signs but usually resulting in an overall milder phenotype (Potocki et al 2000; Potocki et al 2007). According to a systematic clinical evaluation study, PTLS main features are, along with developmental delay and cognitive impairments, hypotonia, failure to thrive (FTT), hyperactivity, anxiety, atypia, autistic traits, obstructive and central sleep apnea (Potocki et al 2007) and sleep deficiencies (Mullegama et al 2017) (Fig.4 bottom plot).

The gestalt of two SMS and PTLS patients and their main clinical features over the years are shown by the figure below (Fig.4).

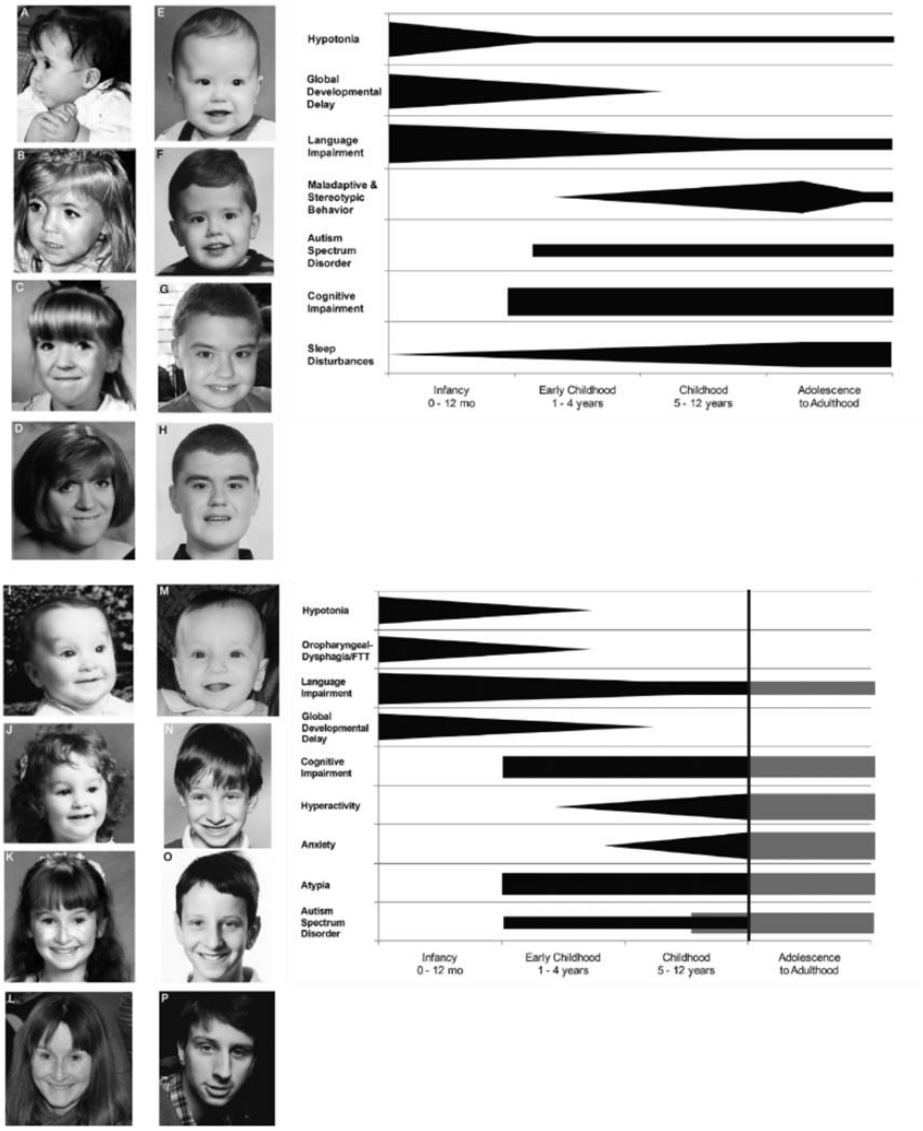

Fig. 4- Gestalt of Smith Magenis Syndrome (A-H) and Potocki-Lupski syndrome (I-P). SMS female (patient BAB 468) 7 months (A), 2 years (B), 9 years (C), 21 years (D). SMS male patient, 23 months (E), 3 years (F), 12 years (G), 17 years (H). Trends of key neurodevelopmental features in SMS throughout age groups (upper righ plot). PTLS female (patient BAB 1006) 8 months (I), 3 years (J), 10 years (K), 28 years (L). PTLS male (patient BAB 1690) 6 months (M), 6 years (N), 10 years (O), 19 years (P). Trends of key neurodevelopmental features in PTLS throughout age groups (bottom right plot). Shaded area represents undetermined prevalence of the PTLS features due to lack of data (Neira-Fresneda, Potocki 2015).

Both SMS and PTLS phenotype emerged with age (Neira-Fresneda, Potocki 2015). As mentioned before SMS individuals, display frontal prominence, synophrys and prognathia (Fig.4 upper left) while PTLS facial features, even if not considered really dysmorphic, consist of inverted triangle shape, down slanting palpebral fissures and relatively small jaw (Fig.4 bottom left). The developmental and behavioural concerns in PTLS as well as SMS seem to shuffle from infancy to early childhood. Cognitive impairment together with autism spectrum disorder

displays a similar trend in both syndromes (Fig.4 plots). Nevertheless among SMS cases autism spectrum disorder is variably represented.

PTLS hyperactivity and SMS maladaptive behaviour seems to escalate from adolescence to adulthood (Fig.4 plots). Sleep disturbance seem to be peculiar of SMS (Fig.4 upper plot), but recently sleep anomalies are observed in PTLS patients too. Hence anxiety and atypia are usually reported in PTLS but not in SMS. Notably due to lack of data, the prevalence of PTLS features in adolescent and adult are not available (Fig.4 bottom plot).

1.1.3_Molecular and genetic basis

SMS is a syndromic congenital disorder due to either a 17p11.2 deletion encompassing retinoic acid-induced 1 (*RAI1*) gene or a mutation in *RAI1*. The 17p11.2 interstitial microdeletion accounts for 90% of SMS cases. A common 3.7 Mb deletion is the rearrangement found in 70% of cases (Shaw et al 2002), while the remaining 20-25% have smaller or larger deletions, also referred as atypical, spanning between 1.5 to 9 Mb.

Recurrent 3.7 Mb microdeletions occur by an aberrant recombination mechanism between region specific DNA blocks (10-400 kb) with a >95% sequence identity known as Low-copy repeats (LCR) or paralogous Segmental Duplications (SD) (Stankiewicz, Lupski 2002), representing almost 5% of our genome.

SD can be inter-chromosomal and intra-chromosomal depending on their chromosomal distribution. The inter-chromosomal LCR/SD are mainly located at either pericentromeric either subtelomeric regions, while intra-chromosomal LCR/SD are peculiar of a specific chromosome.

Chromosome 17p11.2 is one of the highly rearrangement prone region due to the presence of intra-chromosomal SD mediating a Non Allelic Homologous recombination (NAHR) throughout meiotic crossover. Indeed, NAHR underlies common deletion observed in 70% of SMS cases. NAHR between SD typically results in two products, a deletion and a reciprocal duplication of SDs flanked region (Liu et al 2011) (Fig.5, bottom side). Three copies of a low–copy number repeats (LCRs), proximal, middle and distal SMS Repeats (REPs) (Fig.5), flank the SMS deleted region (Chen et al 1997), and two of them, the proximal and the distal SMS REPs, mediates a recurrent about 3.7 Mb deletion occurring by inter- or intra-chromosomal recombination. As expected NAHR mediates the reciprocal dup(17)(p11.2p11.2) including *RAI1*, and resulting in

Potocki-Lupski Syndrome. Noteworthy the incidence of reciprocal duplication remained under-estimated due to both a detection limit and PTLS milder phenotype.

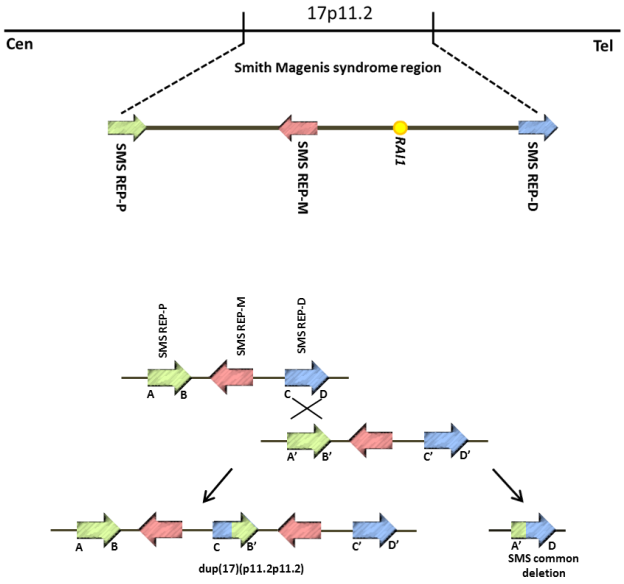

Fig.5- Smith Magenis genomic region structure including *RAI1* gene (yellow dot). 17p11.2 with proximal (SMS REP-P), middle (SMS REP-M) and distal (SMS REP-D) Repeats (upper side); Non Allelic Homologous Recombination occurring between proximal and distal REPs resulting in duplication, dup(17)(p11.2p11.2) and SMS ~4Mb deletion (bottom side). Different colored arrows represent three different REPs and their direction (modified by Potocki et al 2000; Elsea, Girirajan 2008).

Diagnosis of SMS was based on a clinical suspicion and assessed by fluorescent *in situ* hybridization studies (Phenotype First approach), while PTLS diagnosis, as most of microduplication syndromes, is usually reached after a genome wide analysis (Genotype First approach) due to issues in assessing PTLS clinical diagnosis. Indeed, initially the number of SMS clinically reported cases was higher than PTLS (~300 versus just 75 cases, respectively) (Zhang et al 2010). However, once array comparative genomic hybridization allowed an high resolution identification of genomic variants (i.e. microdeletions and microduplications) genotype-phenotype correlation arose and enabled PTLS patients description (Brown et al 1996; Potocki et al 2000; Potocki et al 2007).

The genomic instability of 17p11.2 results from the prevalence of several repetitive elements such *Alu* elements and AT-rich repeats. Hence, the remaining 20-25% of SMS cases display atypical deletions, either larger or smaller than 4Mb, 50% due to NAHR and 50% mainly due to Non Homologous End Joining (NHEJ) (Shaw et al 2004; Shaw et al 2005). Thus corroborates the idea of 17p11.2 as a complex-rearrangement keen on genomic region as shown in Fig.6.

Furthermore, 17p11.2 deletion is typically a *de novo* event, but some familial cases has been observed, for instance, due to a mosaic condition in the mother (Zori et al 1993; Campbell et al 2014).

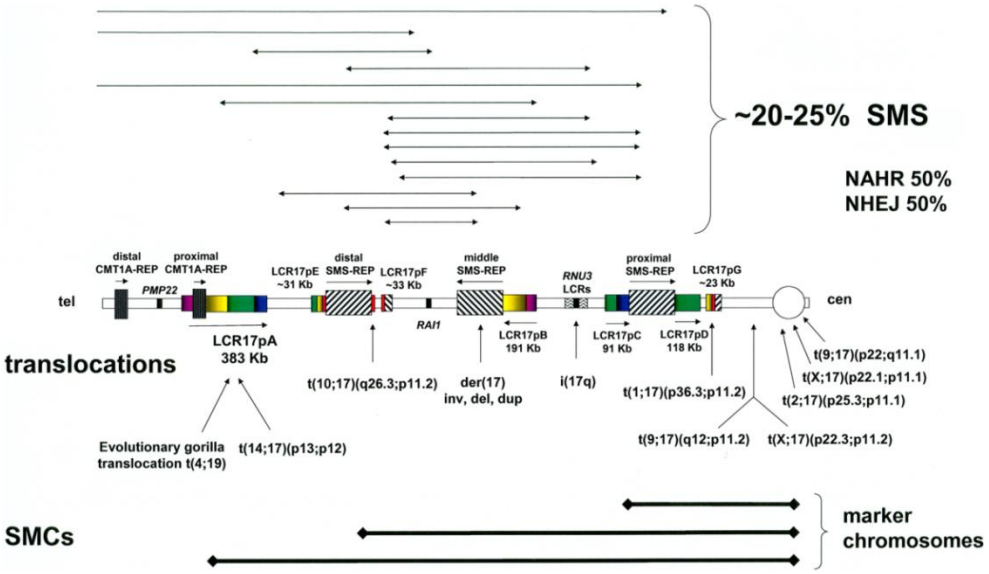

Fig.6- Chromosome 17p non-recurrent rearrangements. Proximal 17p complex genome architecture with several LCRs. LCR are represented by filled color-coded rectangles, hatch pattern and arrows define the orientation. The location of *RAI1* gene and isochromosome 17q breakpoint cluster regions are highlighted. The upper side shows the region involved in SMS patients with atypical rearrangement, arrowheads indicate breakpoints. The bottom side shows the 17p11.2 breakpoints of translocations and the regions contained in the supernumerary marker chromosome (SMCs) (Lupski, Stankiewicz 2005).

Although dissecting the different-sized SMS deletions a common overlap region of 1.5 Mb within 17p11.2 emerged (Slager et al 2003; Vilboux et al 2011). Several known genes were included in this 1.5 Mb critical region and for long time SMS has been considered a contiguous gene syndrome (Greenberg et al 1991). Subsequent sequence analyses of three patients with SMS phenotype, lacking the common deletion, identified frame-shift mutations on *RAI1* gene (Slager et al 2003). Further studies reveal missense, non- sense and in-frame mutations mostly located on exon 3 (Fig.7) and affecting all transcript isoforms, thus making *RAI1* SMS causing gene (Slager et al 2003; Bi et al 2004; Girirajan et al 2005; Bi et al 2006; Elsea, Girirajan 2008; Truong et al 2010; Vieira et al 2012).

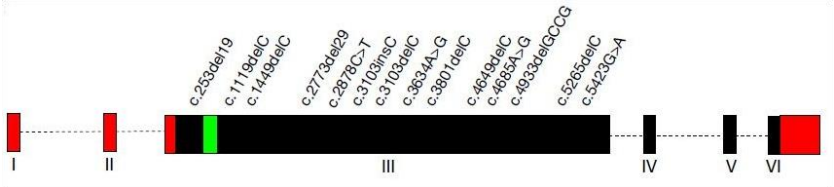

Fig.7- *RAI1* exon 3 mutations hotspot. *RAI1* gene structure with non-coding (red blocks) and coding regions (black blocks). All reported mutations are represented (Adapted from Elsea and Williams 2011).

Among patients with classical SMS clinical features with no 17p11.2 deletion, 10% of cases showed frame-shift and/or truncating mutations in *RAI1* (Slager et al 2003). As shown in Tab.2, most of SMS clinical features are observed in similar percentages in both 17p11.2 deleted and *RAI1* mutated patients. Although short stature, hearing loss, cardiovascular and renal malformation, and obesity resulted differentially represented in patients with 17p11.2 deletion and *RAI1* mutation.

Clinical features	*17p11.2 deletion (%)*	*RAI1 mutation (%)*
Craniofacial/skeletal		
Brachycephaly	>90	81.8
Midface hypoplasia	>90	72.7
Prognathism (relative to age)	>50	88.8
Tented upper lip	70–90	91.6
Broad, square face	>80	90.9
Synophrys	30–65	33.3
Cleft lip/palate	0–10	0
Brachydactyly	>80	83.3
Short stature	>70	9
Scoliosis	40–70	36.3
Otolaryngologic abnormalities		
Chronic ear infections	80–90	54.5
Hearing loss	60–70	10
Hoarse, deep voice	>80	100

Clinical features	*17p11.2 deletion (%)*	*RAI1 mutation (%)*
Neurological/behavioral		
Variable mental retardation	100	100
Speech delay	>90	70
Motor delay	>90	70
Hypotonia	>90	61
Seizures by history	11–30	16.6
Sleep disturbance	>90	100
Self hugging/hand wringing	50–80	100
Attention seeking	80–100	100
Self-injurious behaviors	70–90	100
Onychotillomania	25–85	100
Polyembolokoilamania	25–85	80
Head banging/face slapping	70	90
Hand-biting/self-biting	80	60
Ocular abnormalities		
Myopia	50–60	60
Strabismus	50–80	40
Other features		
Cardiovascular abnormalities	30–40	0
Renal/urinary tract abnormality	15–30	0
Obesity	13	66.7
Dental anomalies	>90	NA

Tab.2- Summary of SMS clinical features, percentages got by data published previously (Elsea, Girirajan 2008). Two columns highlight that most of the signs are equally represented independently of genetic variants underling the SMS phenotype.

Diagnostic iter to detect SMS deletion classically goes through high-resolution karyotype analysis by G-banding and fluorescent in situ hybridization, while multiplex ligation-dependent probe amplification, a-CGH and real-time PCR allow the identification of smaller rearrangements. If no deletions are detected *RAI1* Sanger sequencing is used to assess putative *RAI1* mutation (Elsea, Girirajan 2008).

Notably just 50% of patients with a clinical suspicion of SMS get a molecular diagnosis (Elsea, Williams 2012). Thus it is likely that other loci may contribute to SMS or SMS-like phenotype.

1.2_Disease-causing gene

1.2.1_*RAI1*

*R*etinoic *A*cid *I*nduced gene *1* (*RAI1*) is recognized as the disease-causing gene. The primary transcript for *RAI1* (GenBank AY172136, AJ271790; NM_030665.3; NP_109590.3; OMIM*607642) is formed by six exons, generating an 8.5 kb mRNA and a 1906-amino- acid protein encoded by exons III, IV, V, VI (Fig. 7) (Toulouse et al 2003). RAI1 is a transcriptional modulator involved in cell growth/cell cycle regulation, bone and skeletal development, lipid and glucose metabolisms, embryonic development and neuronal differentiation, behavioural functions, and circadian activity (Girirajan et al 2009; Williams et al 2012; Huang et al 2016). Across vertebrates analysed RAI1 is an ~200 kDa protein containing conserved domains, an N-terminal transcriptional activation domain (TAD) (Bi et al 2005), nuclear localization signal (NLS), polyglutamine and polyserine tracts, and a C-terminal chromatin remodelling plant homeodomain (PHD finger or ePHD/ADD (extended plant homeodomain/ATRX-DMNT3-DNMT3L) domain (Fig. 8)) (Darvekar et al 2013; Tahir et al 2014). C-terminal domain seems to be crucial for nuclear localization of RAI1 protein (Carmona Mora et al 2012). Indeed, SMS patients with either C-term truncating either point mutations involving C-term site display a protein unable to reach nuclear compartments (Carmona Mora et al 2012).

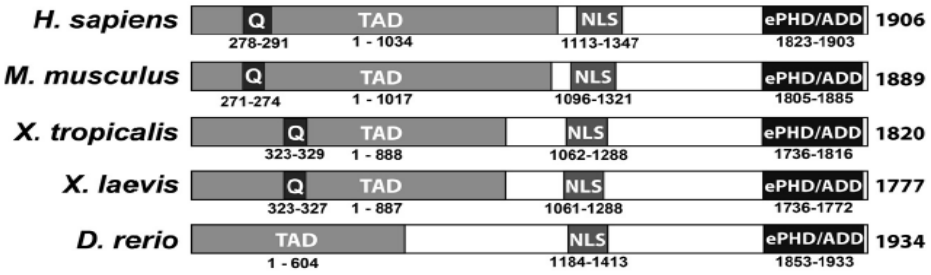

Fig.8- RAI1 protein organization: structural organization of RAI1 functional domains poyQ, TAD, NLS and PHD/ePHD-ADD in *H.sapiens*, *M.musculus*, *X.tropicalis*, *X.laevis* and *D.rerio* (Tahir et al 2014).

Mus musculus protein displays the higher overall sequence and specific domain identity of ~80% compared to human one. Two different species of frogs, *X. tropicalis* and *X. laevis*, share respectively 44% and 42% of sequence similarity with full length human *RAI1* (Tab.3). Hence both frogs species show a 60% sequence similarity within the chromatin interacting ePHD/ADD

domain. Zebrafish (*Danio rerio*) even if the lowest, has a 27% sequence identity with human protein and shares almost 60% similarity by ePDH/ADD domain (Tab.3). These data strongly support an evolutionary conserved role of RAI1 throughout different species.

Species	Percent identity with *Homo sapiens*			
	Full-length	TAD	NLS	ePHD/ADD
Mus musculus	82	85	80	84
Xenopus tropicalis	44	49	42	65
Xenopus laevis	42	49	43	68
Danio rerio	27	35	23	58

Transcriptional activation domain (TAD), nuclear localization containing region (NLS); ePHD/ADD (extended plant homeodomain/ATRX-DMNT3-DNMT3L) domain.

Tab.3- Comparison of human RAI1 full-length protein sequence and major domains with mice, frogs and zebrafish (Tahir et al 2014)

According to murine model studies (Bi et al 2005), *Rai1* expression in brain and craniofacial tissues reflects its relevant contribution to their specific development (i.e. orofacial, neural crest and cartilage). *Xenopus l.* morphants show a reduced size of forebrain ventricle and anomalous nerve tracts likely due to reduced brain derived neurotrophic factor (BDNF) expression (Tahir et al 2014). Further functional analyses reveal a broad expression of *Rai1* in post-mitotic neurons where it acts as a positive regulator of target genes. Rai1 interacts directly with chromatin, preferentially at active promoter and enhancer regions, of genes mainly related in circuit assembly and neuronal communication. Hence, different cell types sense Rai1 loss differentially. Basically Rai1 does not play a general housekeeping function, mandatory for every cell type. Rather, Rai1 has more crucial role in certain cell, i.e. subcortical excitatory neurons, the major contributors of SMS phenotypes in mice (Huang et al 2016).

Animal models support *RAI1* direct involvement as a dosage sensitive gene accounting for most of the clinical signs of SMS and PTLS (Walz et al 2003; Walz et al 2004; Bi et al 2005; Walz et al 2006; Girirajan et al 2008; Ricard et al 2010; Lacaria et al 2013). A growing number of structure/function and phylogenetic data and animal models corroborate RAI1 role as transcriptional modulator involved in neuronal growth and neurobehavioral regulation.

1.2.2_Factors putatively regulating *RAI1* expression

Due to *RAI1* role in brain development, its expression is higher in this tissue (Toulouse et al 2003). Very few is known about its transcriptional regulation, but in a recent study two SNPs,

rs9907986 and rs4925102 in 5'UTR *RAI1* were identified as eventual regulatory elements (Chen et al 2016). Indeed, the SNPs mentioned are supposed to corrupt the binding of DEAF1 transcription factor and RXR-RAR receptor, respectively at *RAI1* 5'-upstream region, accounting for 30-40% of RAI1 expression variance in human prefrontal and temporal cortex (Chen et al 2016).

Regarding *RAI1* post-transcriptional regulation no details are available from literature. Even though within the SMS deletion common overlap region of 1.5 Mb, *SMCR5*, Smith Magenis syndrome chromosome region candidate 5, a non-coding RNA is reported (Bi et al 2002), but its function on *RAI1* modulation remain to be investigated.

As mention before other syndromes show a phenotypical overlapping with SMS, i.e. 2q23.1 deletion syndrome and BDMR syndrome (2q37 deletion), caused by *MBD5* and *HDAC4* genes haploinsufficiency respectively. Indeed, in a recent array CGH screening of 52 SMS-like patients displaying most of SMS clinical features but lacking either the typical SMS deletion either *RAI1* mutation, *HDAC4* and *MBD5* alterations were found (Williams et al 2010 a). Among 52 SMS-like cases, 2 of them have a 2q37 deletion already associated to BDMR, and other 2 of them a novel mutation on *HDAC4* gene. Subsequent RT-qPCR on these 4 patients reveal that, either deletion including *HDAC4* either *HDAC4* mutation results in *RAI1* transcripts downregulation (Williams et al 2010 b), supporting their possible connection and the overlapping phenotypes of SMS and BDMR syndromes.

HDAC4 is a class IIa histone deacetylase, located on 2q37.3 chromosome, made of twenty-seven exons, which raise a 1084 aa protein (NM_006037.3; NP_006028.2; OMIM*605314). HDAC4 regulates transcriptional program essential for synaptic transmission and information processing in the brain. These roles are accomplished by dynamic interactions with transcription factors and neuronal chromatin (Sando et al 2012). Even though it seems to be dispensable for neuroprotection, its truncated form is stably retained in the nucleus of cultured neurons and able to abolish HDAC4 target genes expression (Sando et al 2012). Since BDMR patients show *RAI1* downregulation, might be posited that HDAC4 plays as *RAI1* transcriptional regulator.

The second locus that when disrupted results in SMS-like phenotypes is at 2q23.1 and involves *MBD5* gene (Williams et al 2010 a). Talkowski et al. in 2011 demostrated that 2q23.1 deletion

syndrome results from deletion in chromosomal region 2q23.1 including methyl-CpG-binding domain 5 (MBD5) or *MBD5* gene specific deletions (Talkowski et al 2011). MBD5 is a member of the MBD family and it is expressed in human brain in two isoforms. Translation of exon 6-15 yield the main protein isoform (Laget et al 2010). Unlike others MBD family members MBD5 MBD domain accomplishes interaction with Polycomb repressive complex PR-DUB (Baymaz et al 2014). Mullegama et al. on 2015 assessed a downregulation of *RAI1* in 2q23.1 deletion, thus supporting the idea that also MBD5 might exert a control on *RAI1* transcription (Mullegama et al 2015 a).

Hence further studies correlates *MBD5* haploinsufficiency of patients lymphoblastoid cell line to downregulation of Clock Circadian genes (CCG) (*PER1*, *PER2*, *PER3, NR1D2, CRY2*) as well as *RAI1,* thus linking circadian rhythms impairment to *RAI1* expression (Mullegama et al 2015 b).

Besides, *RAI1* has been genetically linked with schizophrenia (Toulouse et al 2003), autism related condition (Van Der Zwaag et al 2009), and resulted downregulated in multiple intellectual disability syndromes not directly associated with *RAI1* mutations. This suggests RAI1 might act as downstream effector in other neuropsychiatric conditions.

1.2.3_RAI1: a chromatin reader

A label-free proteomics approach (Eberl et al 2013) on mice tissue lysates identified a group of novel reader proteins that specifically recognize unmethylated H3K4. The new so called “RAI1 complex” includes iBRAF (HMG20B) an High Motility Group-box protein that promotes MLL1-mediated H3K4me3 installation, RAI1, PHF14 and TCF20/SPBP.

Notably, as observed for RAI1, TCF20 and PHF14 are linked to neurodevelopmental disorders (NDD) and MLL1, an H3K4me writer that may participate in this complex interacting with iBRAF, is associated with an intellectual disability syndrome (Jones et al 2012). *RAI1* shows >50% similarity with TCF20 gene, a transcriptional cofactor (Darvekar et al 2013). RAI1, TCF20 and PHF14 all share a putative methyl-histone recognition module PHD or extended PHD (ePHD), while iBRAF due to its High Mobility Group domain can bind DNA. Unlike typical chromatin regulatory complexes no histone-modifying enzymes seem to be within this complex. It is likely that according to iBRAF role in MLL1 recruitment, the whole complex act as a reader of combined histone modifications stabilizing MLL1 on specific chromatin areas. The RAI1 complex

binds to unmethylated H3K4 and repelled H3K4me3 (Eberl et al 2013). Basically the unmethylated status serves as a "sensor" to find yet-unmethylated and/or recently demethylated H3K4 residues on gene promoters, thus recruiting MLL1 to tri-methylate H3K4 and prompt gene transcription.

RAI1 complex seems to counteract/counterbalance the activity of a well-known repressor complex, LSD1-CoREST that negatively regulates neuronal differentiation removing histone modifications from neuron specific genes. Specifically iBRAF competes with LSD1-CoREST complex at neuronal gene promoter and/or prevents BRAF35 (its structurally related HMG-box protein belonging to LSD1 complex) sumoylation which is crucial for BRAF35 anti-neurodifferentiation activity (Ceballos-Chavez et al 2012). Overall both the complexes show an activity dependent gene expression essential for learning and memory (Ebert et al 2013) and neuronal plasticity (Loebrich, Nedivi 2009). In a recent *in-vitro* study RAI1 was shown to interact directly with an intronic region 1kb upstream *BDNF* promoter in HEK293T cells, promoting the transcription of a luciferase reporter DNA containing this intronic region. Moreover, Rai1 depletion decreases Bdnf expression in mouse hypothalamus and frog embryonic brain (Bi et al 2005, Tahir et al 2014). These data suggest a tight involvement of RAI1 in *BDNF* transcription, which is a key factor for neuronal development and synaptic plasticity (Loebrich, Nedivi 2009). Finally, can be postulated that RAI1 might trigger an increased *BDNF,* then MLL1 is recruited at neuro-specific gene promoters to tri-metilate H3K4 (Fig.9). Thus activity dependent genes are transcribed.

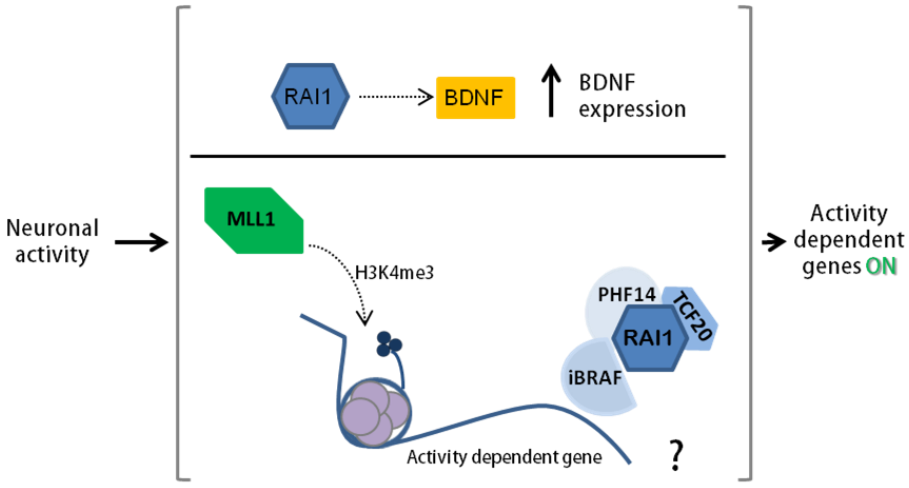

Fig.9-Model of neuronal activity dependent transcription activation (Modified by Garay et al 2016).

1.3_Circadian Clocks & Circadian Rhythms

Circadian rhythms corruption is involved in SMS sleep disturbance phenotype. Williams et al. 2012 demonstrated that *RAI1* haploinsufficiency resulted in a significant impairments of core circadian genes expression pattern thus linking SMS sleep disturbance phenotype to a proper circadian component homeostasis (Williams et al 2012).

Circadian rhythms are 24hrs based biological cycles that enable organisms to adapt their physiology to daily shifts from sunlight to darkness. In mammals the circadian system is hierarchically structured (Albrecht 2012). The light stimulus, as external environment input, is detected by retina, transmitted to hypotalamus suprachiasmatic nuclei "the pacemaker", and spread/transferred to peripheral cells/tissues to elicit a response (Albrecht 2012) (Fig.10).

Each cell contains its clock (Balsalobre et al 1998), thus individual oscillators has to be synchronized and tissues kept in stable phase-relationship with each other. Hence tissues represent an internal environment that in turn might give in information to the clock/pacemaker.

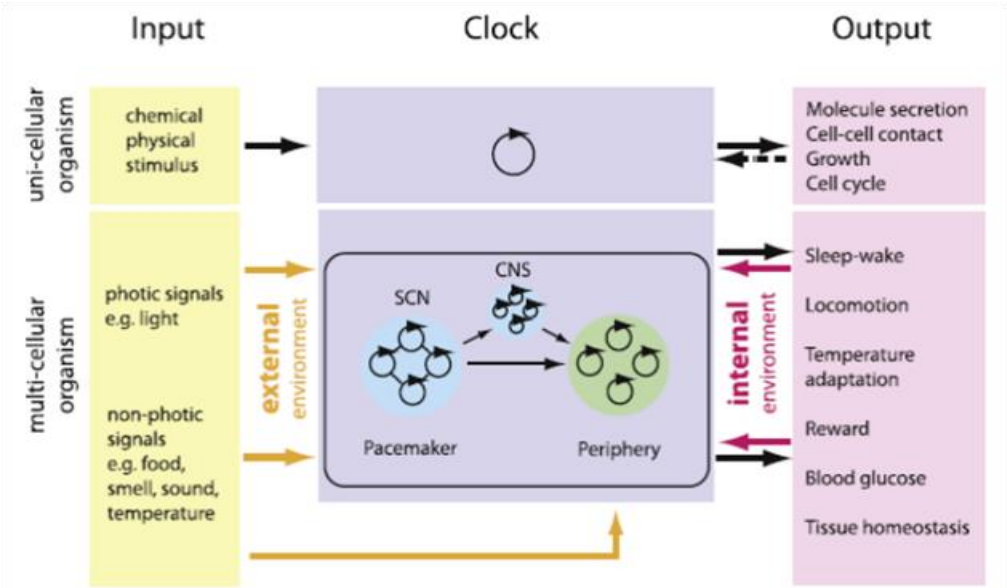

Fig.10- Circadian system structure: input to the clock, clock mechanism and clock output. Upper side represents the division at cellular level, bottom side show the subdivision at systemic level (Albrecht 2012).

1.3.1_Molecular Clockwork

The molecular mechanism that makes the clock work in mammals relies on cell-autonomous oscillator generated by a transcriptional-translational negative feedback loop with a critical delay between stimulus and response (Fig.11). The core clock genes *CLOCK* and *BMAL1* encode for activators (positive elements, Fig.11), and *PER1*, *PER2*, *CRY1* and *CRY2* which encode for repressors (negative elements, Fig.11).

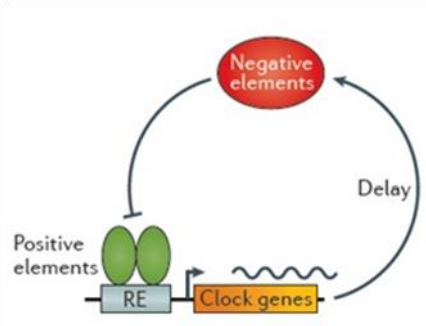

Fig.11- Transcription feedback mechanism of core clock genes. Positive elements (i.e. CLOCK, BMAL1); negative elements (PER1, PER2, CRY1 and CRY2) (Tahakashi 2017).

CLOCK and BMAL1 heterodimerize triggering the expression of "clock controlled genes" (CCG) plus their negative regulators, PER period proteins (PER1, PER2) and cryptochromes (CRY1 and CRY2) (Lowrey, Takahashi 2004; Emery, Reppert 2004). First half of the day is characterized by ascendant transcription of a large number of output genes, then repression by PER/CRY heterodimers and activator transcription is inhibited. The delay in-between these oscillation is guaranteed by post-translational modifications (Fig.11-12). Phosphorylation by Casein Kinases I family, CK1δε allow PER/CRY dimers translocation to the nucleus, where they repress their downstream targets (i.e. CLOCK/BMAL1) (Fig.12). At the end of circadian cycle the PER and CRY proteins are specifically ubiquitilated and degraded by proteasome enabling a next cycle to start (Gallego, Virshup 2007; Lowrey, Takahashi 2011; Preussner, Heyd 2016).

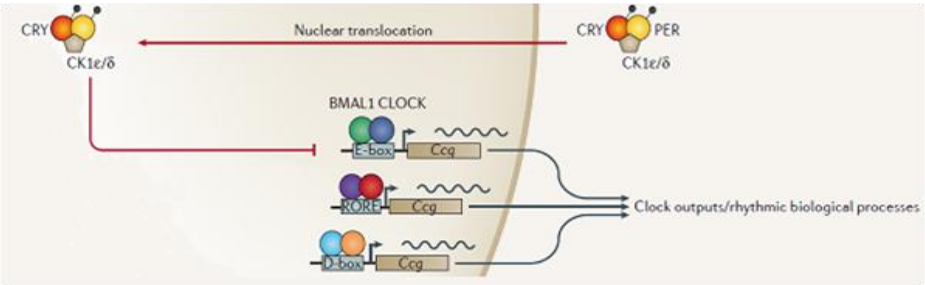

Fig.12- CRY/PER negative transcriptional feedback. CK1δε phosphorilations of CRY/PER heterodimers allow nuclear translocation thus transcriptional repression of *BMAL1/CLOCK*. *BMAL1/CLOCK* repression is a clock output essential to trigger biological processes rhythms (Tahakashi 2017).

According to Ueda et al. 2005, CCG transcription is modulated by three motifs: E-box elements found in clock genes too, Nuclear Responsive elements (NRE) (Ueda et al 2002), and D-box elements (Ueda et al 2005) (Fig.13). Each of them has several regulators involved in the cellular clock machinery modulation and are classified in three groups: E-box regulators (i.e. *CLOCK*, *BMAL1*, *PER1*, *PER2*, *PER3*, *CRY1*, *CRY2*, *BHLHE40*, *BHLHE41*, *NPAS2* and *BMAL2*); D-box regulators (i.e. *DBP* and *NFL3*); and RORE-box/NRE regulators (i.e. *RORA*, *RORB*, *RORC*, *NR1D1*, *NR1D2*).

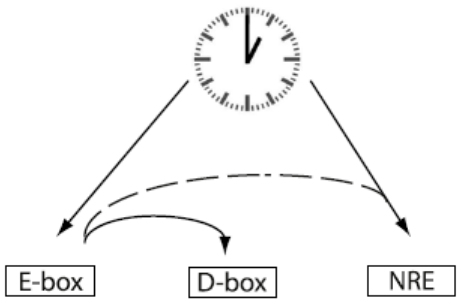

Fig 13- Three promoter motifs regulating clock controlled genes (CCG), direct regulation is represented by black arrow, indirect regulation by hatched line arrow (Abrecht 2012).

Neurodevelopmental diseases (NDDs) are often characterized by sleep abnormalities due to compromised circadian rhythms. SMS and its overlapping syndromes often display a sleep disturbance phenotype. As demonstrated by Williams et al. 2012 a downregulation of main circadian genes cluster in *RAI1* silenced cell line was observed. In particular, both *RAI1* silenced HEK293T and SMS patients fibroblasts display *CLOCK*, *BMAL1*, *PER1* and *CRY1* downregulation. Hence dose-dependent *RAI1* knockdown in U2OS-B cells results in circadian period shortening and dampened *BMAL1* expression, thus mimicking *CLOCK* silencing *in vitro* and further supporting a crucial role for RAI1 in circadian rhythms maintenance. Indeed, RAI1 activates *CLOCK* transcription binding an enhancer element located at *CLOCK* intron 1 directly or within a complex (Williams et al 2012).

Besides, circadian genes regulation is orchestrated by periodic relaxing and compacting of chromatin structure at gene promoters (Ripperger, Schibler 2006). Indeed, dis-regulation of histone methylation likely influences not only cognitive deficits but also sleep-related symptoms in NDDs. Reminiscent of activity-dependent gene expression described in the previous paragraph, H3K4 regulators associated with NDDs could be essential for circadian transcriptional program too.

A possible mechanistic model has been posited to explain *RAI1* role in circadian rhythm (Fig.14). Acetylated MLL1 is recruited at circadian gene promoters by a putative RAI1-complex dependent mechanism, thus allowing circadian genes expression by tri-metilation of their promoters at H3K4. Methyl transferase activity of MLL1 is dynamically regulated by SIRT1 dependent MLL1 de-Acetylation; de-acetylation of MLL1 K1130 and K1133 is supposed to attenuate transcription inhibiting MLL1 activity at promoters (Garay et al 2016).

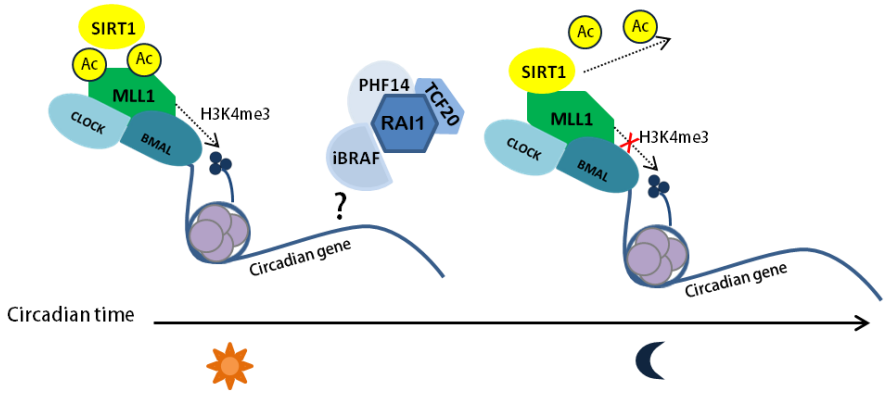

Fig.14- RAI1 and MLL1 in circadian gene expression model (Modified by Garay et al 2016).

AIM

Smith Magenis like syndrome (SMS-like) corresponds to every neurological disorder which clinically resembles Smith Magenis syndrome (SMS) but molecularly lacks the classical microdeletion at 17p11.2 encompassing *RAI1* or mutation in this gene. The difficulty of a proper clinical diagnosis is also emphasized by the later manifestations of the disorders whose clinical traits become more evident during school age. Up to 50% of patients with a suspicion of SMS do not have SMS classical genetic defects, thus it is likely that at genomic level more than one locus is involved in the disorder and may be responsible for similar phenotypes. Actually neither detailed mechanistic insight into RAI1 pathway nor an alternative molecular diagnosis able to explain SMS *RAI1* negative patients phenotypes are available.

Patients with a clinical suspicion of SMS but without a molecular diagnosis should be considered for whole genome high throughput analyses; using array Comparative Genomic Hybridization (array CGH) as primary tool, it will be easy to identify Copy Number Variants (CNVs) potentially containing dosage sensitive genes that, when disrupted, lead to an SMS-like phenotype.

The main goal of this project will be a genetic and functional investigation of candidate genes implicated in SMS-like clinical manifestation.

In a pilot study, a cohort of 40 patients with a clinical suspicion of SMS but without 17p11.2 classical microdeletion was selected. CNV yet unreported in healthy subjects according to the Database of Genomic Variants will be chosen. Functional analysis on the most promising candidate will be performed to assess its pathogenic role and its eventual involvement in SMS-like phenotype throughout a direct or indirect link with *RAI1* disease gene.

This combined genomic and functional approach should shed light on still unknown pathways linked to *RAI1*, thus improving both molecular and clinical diagnosis of SMS/SMS-like phenotypes.

MATERIALS AND METHODS

3.1_SMS/SMS-like experimental flowchart

The cohort of cases collected includes 40 SMS-like patients resulting negative to preliminary diagnostic flowchart (Fig.15). In detail, these patients were negative to 17p11.2 deletion (by FISH or low resolution array CGH), *RAI1* mutation (Sanger sequencing), *RAI1* microdeletion (MLPA), and *RAI1* transcripts downregulation (RT-qPCR) (left side of flowchart, Fig.15).

In order to identify CNV potentially containing dosage sensitive genes that when disrupted might lead to patient SMS-like phenotypes high resolution array CGH analysis was performed for all patients. This approach has become an important tool in the genomic evaluation of many CNV-associated diseases (Williams et al 2010 a). Since 50% of SMS patients do not have a molecular diagnosis it can be useful to identify new candidate genes possibly implicated in the same pathways of *RAI1* and thus explaining SMS-like phenotypes.

Genome scan was performed on patients and their parents, by oligo-aCGH Agilent 400K platform, including 420,288 oligonucleotide probes 60nmer long, with a 5 kb spacing on average and 20 kb resolution. CNV yet unreported in healthy subjects according to the Database of Genomic Variants (http://dgv.tcag.ca/dgv/app/home) were chosen. The detected submicroscopic gains or losses were then confirmed by parents analysis or, if necessary, by quantitative PCR.

Meanwhile the phenotypical overlapping genes (i.e. *MBD5* and *HDAC4*) have been screened for mutational analysis by Sanger Sequencing to rule out/switch to a differential diagnosis chance. The detailed experimental workflow is summed up above (Fig.15).

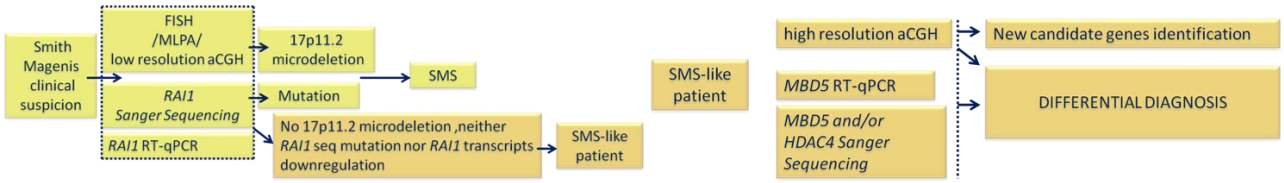

Fig.15- Experimental workflow

3.2_Ethical approval

The study has been approved by Ethics Committee and all the patients included signed an informed consent.

3.3_DNA extraction

Whole blood samples from each patient and their relatives (when available) were collected by EDTA tubes (Beckton Dickinson) and extracted according to GenElute^{TM} Blood Genomic DNA kit protocol (Sigma Aldrich). The DNA was then quantified by NanoDrop (NanoDrop1000, Thermofisher Scientific) and stored at -20C°.

3.4_HUMARA assay

Genomic DNA of each individual was amplified in the Human Androgen Receptor (HUMARA) locus on X chromosome, either without enzymatic digestion (Undigested DNA) and after digestion with *HpaII* (*HpaII* digested DNA). The presence of two X chromosomes with a different number af CAG repeats inside HUMARA alleles results in the generation of two amplicons represented by the peaks. Amplicon size is indicated in bp. The 275 bp amplicon identifies the X chromosome allele that is inherited within the family. The X Chromosome Inactivation (XCI) percentage is established after the digestion with *HpaII*. In women only one of the two X chromosomes is active, thus *HpaII* sites are susceptible to digestion and PCR fails to amplify such allele giving a smaller peak than its undigested counterpart. Peak height is indicated in Relative Fluorescence Units (RFU). Quantification of peaks heights by GeneMapper software was used to calculate XCI percentage after digestion. As control, the patient DNA with only one active X chromosome is completely digested by *HpaII* and gives no amplification. Skewed or random XCI is defined using an arbitrary cutoff of 70-75% of cells with the same X inactivated.

3.5_PCR

The entire 3'UTR and coding regions of *ZDHHC15* and at least 30 bp of the flanking intronic sequences were amplified by polymerase chain reaction (PCR) using AmpliTaq Gold (Applied Biosystems) or Kapa2G Robust PCR Kit (KAPABiosystems). Amplification primers are shown in Tables below (Tab.4-5).

Tab.4- *ZDHHC15* primers

GENE	Exon	Primer sequence (5'→3')	Amplicon size (bp)	Annealing Temp (°C)
ZDHHC15	1	Fw: GCTCCAACATGGCTAGTTCC Rev: AAGGGACACCAGTGTGAAGG	438	59
	2	Fw: CTTGCCTTCCCTCATCTTTG Rev: TGGGAAAATTGCTCGGTCTA	301	56
	3	Fw: TGGCTTGTTTCTGTCACTGTATG Rev: CCTCTTTTTGTCCTCTTCTTGC	346	58
	4	Fw: CCTGAGCTTCAAGGGTAGGT Rev: GGTTTTCAGAAGATGGGAGGA	347	58
	5	Fw: TGTAGTCTGCCTTTTGCTTGG Rev: GTGTGAGGGGTTTTGGCATA	361	57

	6	Fw: GGCCACAGTTTTGGAGTCAC Rev: AATGTTACCCCTCCCCTGTC	335	59
	7	Fw: CGACACATAATGAAGCAGCAG Rev: CACAAGTTGGAGTGGGTGTG	295	58
	8	Fw: AGCACACTCACAGGTATCATCA Rev: CACAGGTCCCTCTGATACACA	372	59
ZDHHC15	9	Fw: TGTGCTACCACAGCAAAAAGA Rev: TGGACTGATACCTGCTGCAT	355	56
	10	Fw: CCATTCCACCATGGCTTTAG Rev: CCACCATCCAGAGGACACTT	355	58
	11	Fw: TCTGTTGCCTGCAGAGATTG Rev: CACACTGCCAAGGGAAATTA	360	56
	12	Fw: CAAGTGGGTGTTACCACATGA Rev: TCCCTTCAACACCAAAAAGG	455	56

Tab.5- *ZDHHC15* 3'UTR primers

GENE	3' UTR fragment	Primer sequence (5'→3')	Amplicon size (bp)	Annealing Temp (°C)
	1	Fw: TTGCTGTGTAAATGTTTCTGGA Rev: GCTGTACGTGTTCACAAATGC	313	56.5
	2	Fw: CCCAATCCATGAAAGCCTAA Rev: CTGTGGTGCTTTCAGGAACA	438	56.4
	3	Fw: TTTGAATCATCGCTATATCAAGTATC Rev: TCTGAAAACCCTTAACAAAACC	591	56.7
	4	Fw: GGGTGCAGTAAAATTCTCCAA Rev: ATTAGTAAGCCAAACCATCCCTCT	592	55.1
	5	Fw: TTGCATCAATTTCCCCATTT Rev: TTGAAACCCAGTGTGTGCAT	559	53.1
	6	Fw: TGACCAAGGTGAGACTTTTGG Rev: TTGACTTCTGTGGGAGCTGA	502	57.5
ZDHHC15	7	Fw: CATCTTCTGCCAAGCATTCA Rev: CCCCTGGTAAAACCCTGATT	578	56.2
	8	Fw: GGAGTGTTGGTGCATGACTG Rev: TGACATAGCACCCTTCAGCA	518	58.2
	9	Fw: TGGATCCCTGTCCAATAACC Rev: ATGGGGCTAGTAGGGGAAAG	619	58.2
	10	Fw: CAGGATCACATTCTGAAAGAGTCA Rev: TGTTCTTCACATGCTGTGTTTC	601	57.5
	11	Fw: CATACACATTTTCTCCAAAGCA Rev: TGCTGATGGCTGTGTACCAT	512	55.8
	12	Fw: CCATATTAAATTGTAGCCTTTTGC Rev: CGCATACCAATCAACCTGAG	499	56.3

3.6_Sanger Sequencing, Sequence purification & alignments

The PCR products were subsequently column purified by Illustra^{TM} GFX^{TM} PCR DNA and Gel Band Purification Kit (GE Healthcare) to remove unincorporated primers and dNTPs, and then sequenced using the BigDye Terminator v3.1 Cycle Sequencing kit (Applied Biosystems). Sequence were purified by Centri-Sep kit (Princeton Separation) and run on Genetic Analyzer 3500 capillary sequencer (Applied Biosystems). All sequence were aligned by ChromasPro software to a wild type (WT) sequence. Detected variants were analyzed by Ensembl (https://www.ensembl.org/) and dbSNP (https://www.ncbi.nlm.nih.gov/projects/SNP/) databases.

3.7_RNA extraction

Each blood sample has been collected in Tempus Blood RNA Tubes (Applied Biosystems) and processed according to Tempus Spin RNA isolation Reagent Kit (Applied Biosystems). The RNA was then quantified by NanoDrop and stored at -80°C until used.

3.8_RT-qPCR

Retrotranscription of 500-800 ng of total RNA samples extracted from whole blood of either patients either controls was performed using High Capacity cDNA Reverse Transcription Kit (Applied Biosystem). Quantitative Real-Time PCR has been performed using *RAI1* TaqMan probe (Hs01554690_m1) and *ZDHHC15* TaqMan probe (Hs00327516_m1). All samples were run in triplicate processed by ABI PRISM 7900HT and normalized to *GAPDH* TaqMan probe (Hs99999905_m1), *TBP* TaqMan probe (Hs00427620_m1), *RPLP0* (Hs99999902_m1) and *HMBS* TaqMan probe (Hs00609297_m1). Differences in transcripts levels quantified by $2^{-\Delta\Delta Ct}$ method. Statistical analysis applied was One Tailed Student T-test.

3.9_Digital PCR

Digital PCR analysis has been performed thanks to a collaboration with Humanitas Research Center.

3.10_Protein extraction from peripheral blood

Leucocytes fraction has been isolated from each blood sample using CPT vacutainer (Beckton Dickinson). The cell pellet was then washed with ice cold PBS and lysed by RIPA buffer (50mM Tris HCl pH 7.4; 1% NP40; 0.5% Na-deoxycholate; 150mM NaCl; 1mM EDTA; 0.1% SDS) plus cOmplete protease inhibitor cocktail (Roche) added just before use. All the RIPA whole cell extracts were stored at -20C°.

3.11_WB analysis

RIPA extracts were loaded on Novex® Tris-Glycine 4-12% acrylamide gel (Thermofisher Scientific), semidry transferred on iBlot® transfer stacks by iBlot®transfer device (Thermofisher Scientific) and immunoblotted with GAPDH ab (NB300-320), ZDHHC15 ab (NBP1-82014). Bands revealed by respective secondary antibodies (peroxidase-mouse anti-goat 200-035-308, Jackson Immunoresearch; goat anti-rabbit ab6721) after 5 mins incubation with Luminata Classico (Millipore).

3.12_HEK293T: culturing methods

HEK293T cells were grown in Dulbecco's Modified Eagles Medium (DMEM) supplemented by 10% Fetal Bovine Serum (FBS, Sigma), 1% penicillin/streptomycin, 1% glutamine and 1% sodium pyruvate at 5% CO_2. HEK293T were maintained according to specific cell line requirements.

3.13_Plasmids creation & selection for luciferase reporter assay

Both *ZDHHC15* 3'UTR wild type and mutated sequences (321 bp) have been amplified by PCR with specific primers, *ZDHHC15* forward 5'-CCTCCCATGAGGCTTACAGA-3' and *ZDHHC15* reverse 5'-GGGGGAATTAAAGACTCTAAGGA-3' at 58.9°C annealing temperature using as templates respectively a control patient DNA and DNA from patient with *ZDHHC15* 3'UTR transversion. Both amplification products were subsequently cloned by TOPO® TA Cloning® Kit into Topo®TA® plasmid (pCR™II-TOPO® vector) according to manufacturer protocol (Thermofisher Scientific). After transforming by heat shock procedure *E.coli* positive colonies selected by IPTG:X-Gal were picked and the insertion direction of fragments was verified by DNA sequencing using BigDye kit (Applied Biosystem). Plasmids isolation was performed by midi prep procedure (Qiagen) and TOPO-TA plasmid constructs were enzymatically digested by *SacI* and *XbaI*. Then wild type and mutated *ZDHHC15* 3'UTR sequence were *SacI* and *XbaI* cloned into pmirGLO dual-luciferase vector (Promega) at 3' end of the firefly gene. All clones and their orientation were validated by DNA sequencing as above.

3.14_miRNAs selection

Different prediction softwares, i.e. miRdb (Wang, El Naqa 2008), DIANA (Kirakidou et al 2004), miRanda (John et al 2004), Target Scan (Lewis et al 2005), miRdb custom, Find Tar3 and RNAhybrid (Rehmsmeieret et al 2004) were used to select miRNAs putatively interacting with *ZDHHC15* 3'UTR. In particular miRdb (http://mirdb.org), DIANA (http://diana.cslab.ece.ntua.gr/) miRanda (http://www.microrna.org) and Target Scan (http://www.targetscan.org) tools enable to choose miRNAs interacting with *ZDHHC15* 3'UTR wild type sequence. Whereas miRdb custom (http://mirdb.org) and Find Tar3 (https://bio.sz.tsinghua.edu.cn/) allowing 3'UTR mutated sequence uploading, shortlisted miRNAs supposed to be specific for *ZDHHC15* 3'UTR mutated sequence. RNA hybrid (http://bibiserv.techfak.uni-bielefeld.de/rnahybrid) has been used to validate the predictions for mutation specific miRNAs on thermodynamic and statistical modeling basis. All predictions were integrated with text mining to shortlist the most relevant miRNAs.

3.15_Co-transfection

HEK293T cells were maintained in 12-well plates according to standard practice. Transfections with a final concentration of 250ng of wild type or mutated *ZDHHC15* 3'UTR pmirGLO constructs and 50nM of each specific miRNA, i.e. hsa-miR-142-5p, hsa-miR-5590-3p, hsa-miR-4797-5p, hsa-miR-191-5p, hsa-miR-922 (qiagen) and miRIDIAN microRNA mimic negative control (Thermofisher Scientific) were performed with Lipofectamine™ 2000 (Thermofisher Scientific) following manufacturer instructions. The cells were then incubated 24hrs at 37C° in 5% CO_2 before harvesting for luciferase assay.

3.16_Luciferase assay

After plasmid and miRNA co-transfection and 24hrs incubation, the samples were washed with Phosphate Buffered Saline (PBS) and lysed in recommended volume of Passive Lysis Buffer included in Dual-Luciferase® Repoter Assay Kit (Promega) following manufacturer protocol. Using a multi-sample luminometer (Fluoroskan Ascent FL, ThermoLabsystems) 20ul of each lysates was dispensed in 96-well plate, nunclon Delta white microwell SI (Nunc) and LAR II solution and Stop&Glo® Reagents set up to be sequentially auto-injected by the device (i.e. 2 seconds pre measurements delay followed by 10 seconds measurement period for each reporter assay). All the measurements were performed according to standard manufacturer protocol (Promega).

The firefly luciferase activity of wild type and mutated *ZDHHC15* 3'UTR constructs was normalized against the renilla luciferase output of the same pmiRGLO construct. Normalized firefly luciferase activity was represented relative to miRNA negative control transfected cells. Statistical analysis applied was One Way Anova and Tukey post-hoc test.

3.17_BE(2)-M17: culturing methods

BE(2)-M17 were grown in Roswell Park Institute Memorial medium (RPMI 1640, Sigma Aldrich) supplemented by 10% FBS, 2% glucose, 1%Sodium Piruvate, 1% penicillin/streptomycin and 1% L-glutamine. BE(2)-M17 were maintained according to specific cell line requirements.

3.18_Gene silencing

BE(2)-M17 were maintained in 6-well plates according to standard practice. For gene silencing experiments the following siRNA duplexes were used: stealth RNAi Negative control medium GC as negative control (Thermofisher Scientific); 5'-GCUGCCGCUUGAGAGAACACUCAAA-3' and

5’-UUUGAGUGUUCUCUCAAGCGGCAGC-3’ for *RAI1*_HSS116567 (Thermofisher Scientific); 5’-GCUACCGGUUUACACAAGAACUGGA-3’ and 5’-UCCAGUUCUUGUGUAAACCGGUAGC-3’ for *ZDHHC15*_HSS136141 (Thermofisher Scientific). Cells were transfected twice, using Lipofectamine™ 2000 (Thermofisher Scientific) with 80nM of the indicated siRNAs duplexes, once every 24hrs and harvested at different time points: 48hrs post the first transfection for siRNA against *ZDHHC15* and its negative control, 96hrs post the first transfection for siRNA against *RAI1* and its negative control.

3.19_RNA extraction: Tri Reagent

BE(2)-M17 cells transiently transfected were lysed and RNA was extracted by Tri Reagent® as described by manufacturer protocol (Sigma Aldrich). RNA obtained were resuspended in DEPC treated water, quantified by nanodrop and stored at -80C°.

3.20_RT-qPCR

Retrotranscription of 3µg of mRNA samples derived from *ZDHHC15* and *RAI1* silenced BE(2)-M17 cells was performed using SuperScript II RT (Invitrogen). Oligonucleotide pairs for each gene were designed with Primer3 4.0 software (http://bioinfo.ut.ee/primer3-0.4.0/primer3/) on exon boundaries. Primers sequences are listed in the table below.

GENE	Primer sequence (5'→3')	Amplicon size (bp)
HDAC4	Fw:TGAGTTCCAGAGGCAGCAC Rev: GCATCTCCTGTTGTTGCTTG	83
MBD5	Fw: CCAGTGATACCAAACAGCATTG Rev: ATGGCTATGGAGGATGATGG	86
SIRT1	Fw: CCTCCTCATTGTTATTGGGTCT Rev: GAGGCACTTCATGGGGTATG	80
ZDHHC15	Fw: CTGGAAGTGGAGCTGTACGA Rev: CACACATAGCACAGACAGAGCA	87
RAI1	Fw: AAAGGGAGACGGCGAGAC Rev: CATGACTCGGGCTGGTTATC	78
CLOCK	Fw: TGCACTGTTGAAGAACCCAAT Rev: GGTGGTGCCCTGTGATCTA	86
BMAL1	Fw: GCGGCTCATAGATGCAAAA Rev: CGTCGTGCTCCAGAACATAA	84
BMAL2	Fw:TGGATGCTTACCCAACTCAA Rev: GGAGGCCAGCTTCTCAAGTA	84
PER1	Fw: TCTGCCGTATCAGAGGAGGT Rev: CCCGGATCTTGGTCACATAC	87
PER2	Fw: CATGTGCAGTGGAGCAGATT Rev: TTCATTCTCGTGGCTTTTCC	94
PER3	Fw: CGGTTACAGCAGCACCATT Rev: GTCCAGGGCTCACAGAAGAG	78
CRY1	Fw: CAGGTTGTAGCAGCAGTGGA Rev: TGTCGCCATGAGCATAGTGT	66
CRY2	Fw: AGGGAGGAGAGACAGAAGCTC Rev: AGGGAGTTGGCGTTCATTC	100
NR1D1	Fw: ACAACACAGGTGGCGTCAT Rev: TAGAGGGATTCAGGGCTGGT	76

NR1D2	Fw: AGGCTGTAAGGGTTTCTTTCG Rev: TTCATTCTTCAGGCACTTCTTG	70
FBLX3	Fw: AGCTACCCATCCAGAGCTGA Rev: AGCTGATTCCTTGCTGCTGT	97
CSNK1D	Fw: CAAAACCGTCCTGCTGCT Rev: AGGAAGTTGTCTGGCTTCACA	99
CSNK1E	Fw: CGTCTTTGACTGGAACATGC Rev: CTCTCCTCGCGTTCGTGT	90
RORC	Fw: GTCCCGAGATGCTGTCAAGT Rev: GCTGTTTCTGCACTTCTGCAT	77
RPL10a	Fw: GAAGAAGGTGTTATGTCTGG Rev: TCTGTCATCTTCACGTGAC	57

Quantitative Real-Time PCR was performed for 40 cycles with SYBR Green PCR Master mix (Applied Biosystems) and processed on ABI PRISM 7900HT (Applied Biosystems). Reactions were run in duplicate for each sample and a dissociation curve was generated at the end. Threshold cycles (Ct) for each tested gene were normalized on the housekeeping *RPL10a* gene value (ΔCt) and every experimental sample was referred to its control (ΔΔCt), fold change values were expressed as $2^{-\Delta\Delta Ct}$. Statistical analysis applied was One Tailed Student T-test.

3.21_CSS-Palm 4.0 software: palmitoylation prediction software

CSS-Palm software (http://csspalm.biocuckoo.org/online.php) allows palmitoylation prediction of target proteins by a clustering and scoring algorithm (Zhou et al 2006). Fasta sequence of each protein of interest has been used to predict eventual palmitoylation sites. *In silico* analysis was performed with a medium threshold. The results obtained are summarized in tabs.

RESULTS

4.1_Preliminary data

Among 40 SMS-like patients array CGH analysis on blood extracted DNA identified a CNV, specifically a deletion on Xq13.3 (chrX:74772380-74826319, hg19) in one male patient (SMS1) inherited from his healthy mother (Fig.16).

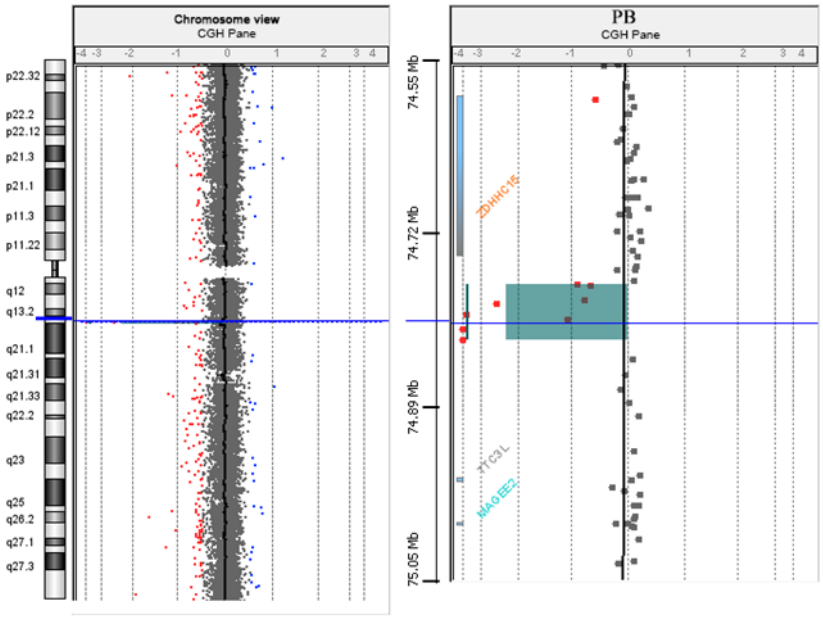

Fig.16- High resolution 400K array CGH analysis (Agilent technology) identified a rare 54 kb deletion in Xq13.3 in SMS1 (chrX:74772380-74826319, hg19).

Patient SMS1 carrying the Xq13.3 deletion is a boy aged 4 years, born from healthy non-consaguineous parents, who came to the attention of the medical geneticist for a suspected genetic syndrome. Clinical evaluation showed in the proband mild craniofacial anomalies such as brachycephaly, square face, thick eyebrows, hypertelorism, and broad palate. Brachydactyly of hands and feet was also noted, as well as generalized hypotonia, developmental delay, behavioural problems (self-injurious), sleep disorders and congenital heart defect that was surgically corrected at age of 1 year. Based on SMS1 clinical evaluation SMS-like suspicion was assessed and according to preliminary diagnostic flowchart (Materials and Methods, fig. 15), 17p11.2 deletion and *RAI1* sequence mutation were excluded. Moreover, SMS1 *RAI1* levels resulted normal compared to ten healthy controls with both *TBP* and *GAPDH* housekeeping genes used to normalize the samples (Fig.17).

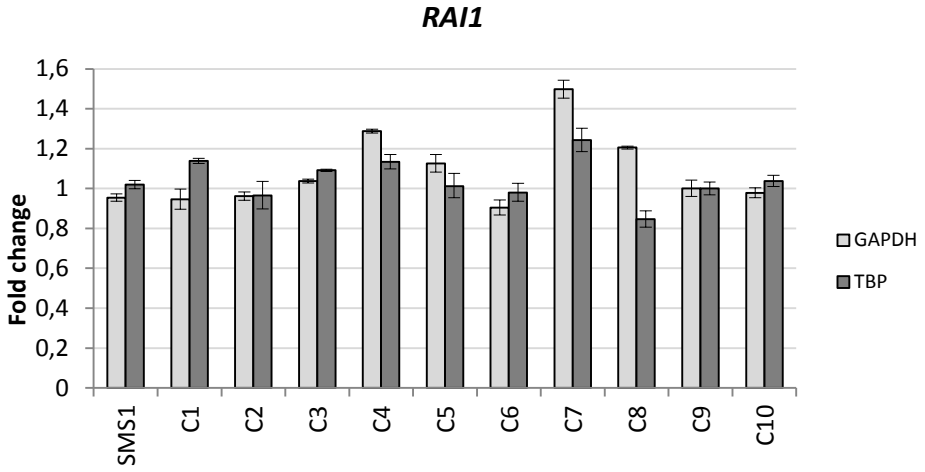

Fig.17- RT-qPCR of *RAI1* expression on SMS1 and ten healthy controls (C1-C10), C1-C5 are female controls, C6-C10 are male controls. RT-qPCR was performed twice using two different housekeeping genes, *GAPDH* and *TBP*.

Array CGH analysis, extended to healthy grandparents and healthy uncle both on mother side, showed that the rare Xq13.3 deletion was not present in the males of the family analyzed but inherited from the grandmother (Fig.18), supporting a possible pathogenic role of this CNV.

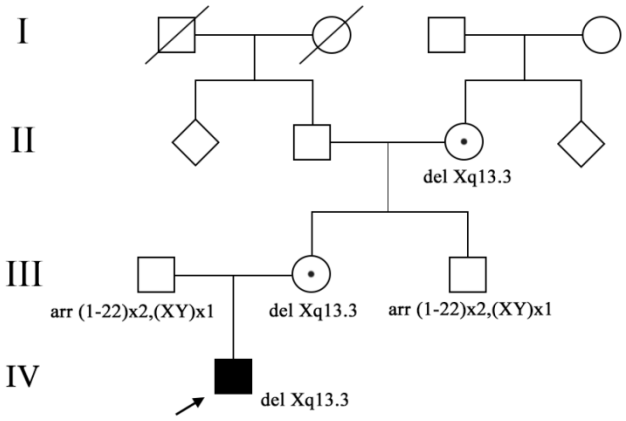

Fig.18- Pedigree representing the inheritance of the CNV identified in SMS1 (filled symbol and highlighted by arrow) among the four generations (I, II, III and IV). Both his healthy mother and maternal grandmother bear the same rearrangement (spotted circles). Array CGH results are indicated for the relatives analyzed.

Human Androgen Receptor (HUMARA) Assay was then used on DNA from peripheral blood lymphocytes to establish the X inactivation pattern in the females of SMS1 family bearing the Xq13.3 deletion. The analysis revealed a skewed X inactivation in the mother (73%-27%) and a random one in the grandmother (38%-62%) (Fig.19). Notably, the skewed allele (275 bp) is the one transmitted to SMS1.

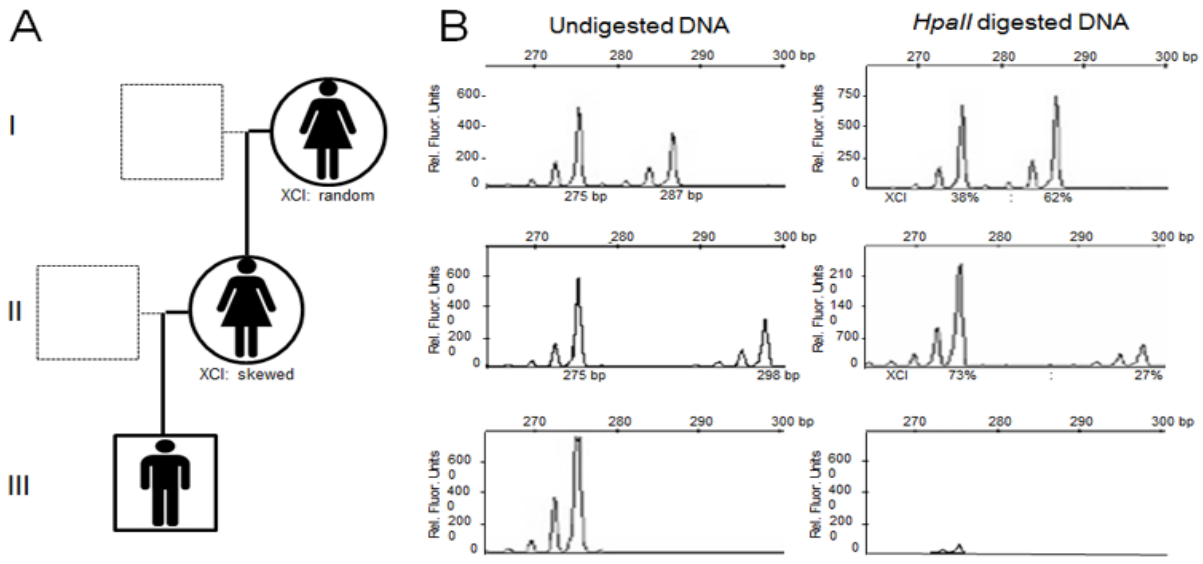

Fig.19- HUMARA assay results. A) Schematic family pedigree showing segregation of the amplified X chromosome allele (275 bp) among the three represented generations (I, II and III). Lines in bold indicate the segregation of the trait in the family; dotted empty squares represent not analyzed males. B) Electropherograms resulting from HUMARA assay. The 275 bp amplicon identifies the X chromosome allele that is inherited in the family (higher peak). The X Chromosome Inactivation (XCI) percentage is established after the digestion with HpaII. Peak height is indicated in Relative Fluorescence Units (RFU). XCI percentage is reported under the peaks. Skewed or random XCI is defined using an arbitrary cutoff of 70-75% of cells with the same X inactivated.

4.2_CNV characterization: are there any genes involved in?

The Xq13.3 deletion spans 54 kb and does not involve any gene but contains a highly conserved region and a predicted insulator (Fig.20). Notably the Xq13.3 deletion maps 29 kb far from the 5' end of *ZDHHC15* (Zinc Finger DHHC domain-containing protein 15) (Fig.20) which encodes for palmitoyl-transferase 15 ubiquitously expressed, but highly expressed in the brain. Moreover, based on literature data, *ZDHHC15* was found previously associated to a nonsyndromic X-linked intellectual disability (Mansouri et al 2005).

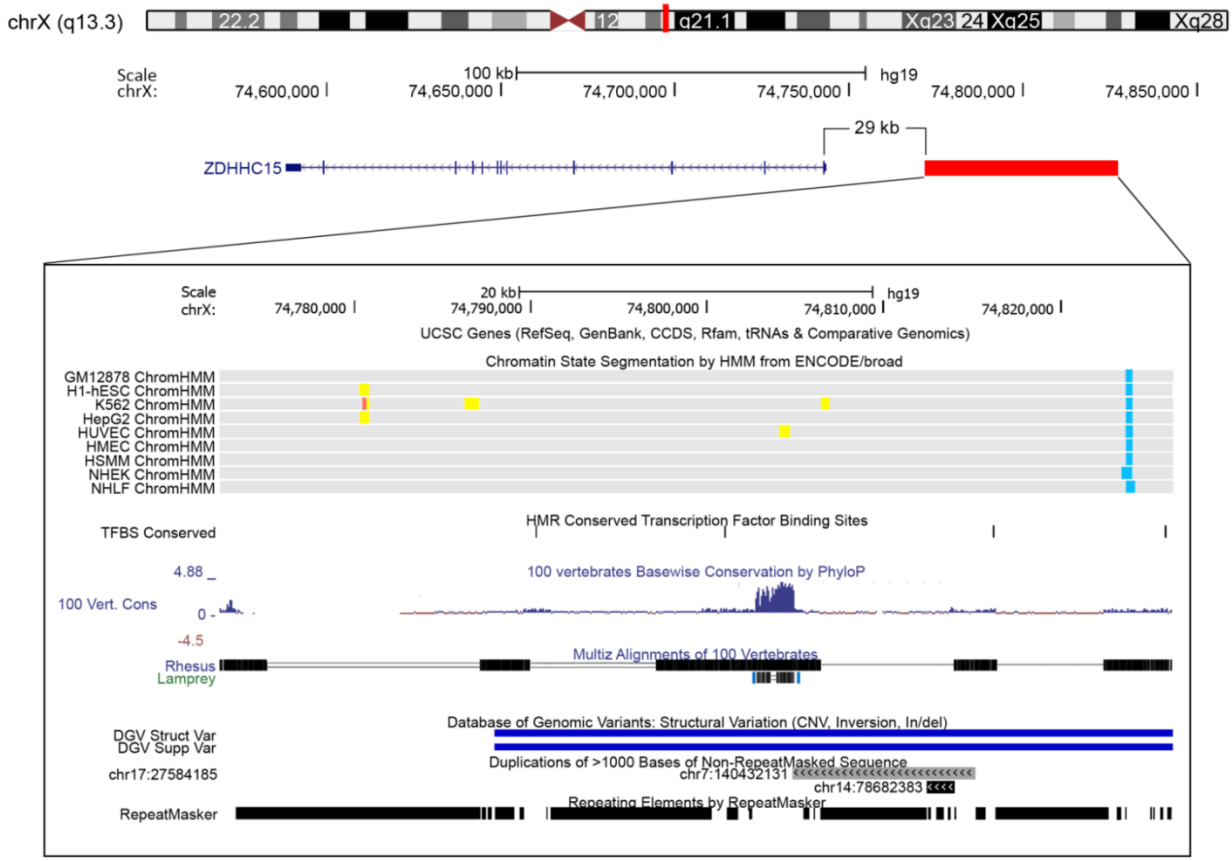

Fig.20- Deleted region on chromosome Xq13.3 is shown by a red bar. UCSC view is represented below. The predicted insulator element is shown by light blue blocks (UCSC, Genome Browser; http://genome-euro.ucsc.edu, hg19).

According to these findings *ZDHHC15* was considered an interesting gene possibly implicated in patient phenotype onset. Hence we hypothesized that the 54 kb deletion involving predicted insulator element might result in *ZDHHC15* transcript alteration by a position effect.

4.3_Could a *ZDHHC15* defect be implicated in the onset of the proband phenotype?

4.3.1_Position effect evaluation by RT-qPCR

To disclose an eventual pathogenic effect of the CNV identified we performed RT-qPCR analysis on peripheral blood RNA of SMS1 and his healthy mother looking for eventual *ZDHHC15* expression changes. RT-qPCR revealed a significantly reduced level of *ZDHHC15* mRNA in SMS1 patient when compared to nine healthy controls, while SMS1 mother *ZDHHC15* levels are similar to controls level (Fig.21, upper panel). The RT-qPCR on SMS1 was then replicated two times with different housekeeping (i.e. *TBP* and *HMBS*) and confirmed a significantly *ZDHHC15* downregulation when compared to ten healthy male controls (Fig.21, bottom panel).

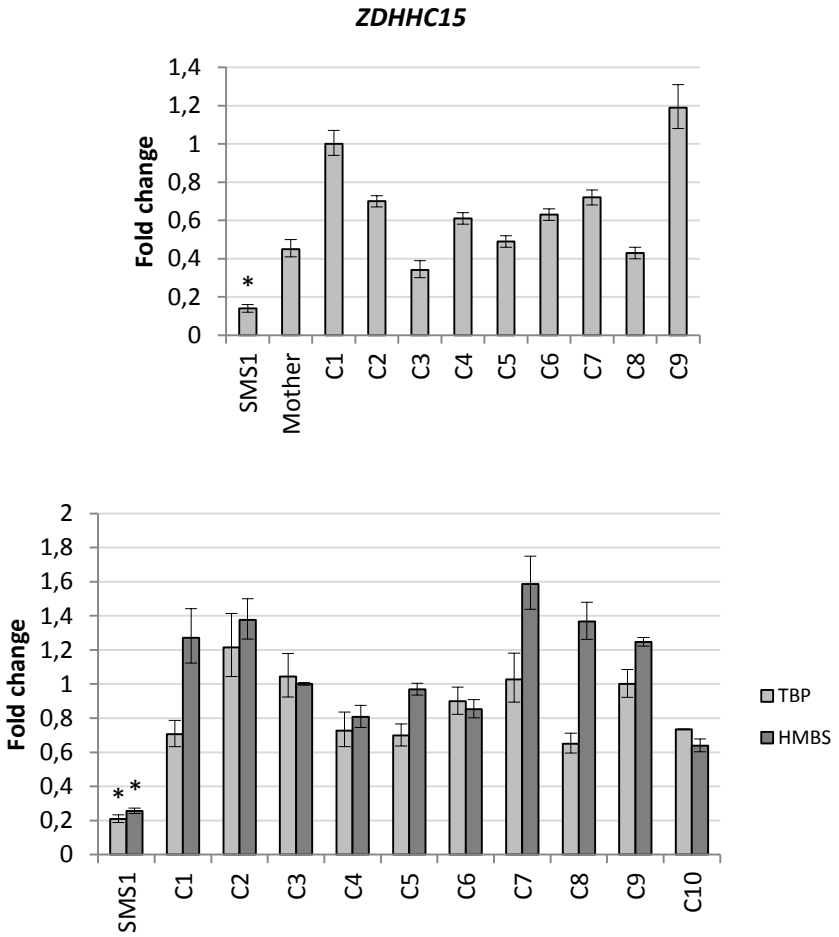

Fig.21- RT-qPCRs analyses of *ZDHHC15* expression on SMS1. Upper panel represents RT-qPCR performed on SMS1, his mother, five healthy male controls (C1-C5) and four healthy female controls (C6-C9), normalized on *GAPDH* gene. Bottom panel represents RT-qPCR performed on SMS1 and ten healthy male controls (C1-C10) normalized on *TBP* and *HMBS* genes. Student T test, *P<0.01.

4.3.2_Is *ZDHHC15* a candidate gene?

Findings obtained on SMS1 and *ZDHHC15* association with X-linked intellectual disability (OMIM #300577, MRX91) prompted us to Sanger sequence *ZDHHC15* in all SMS-like male patients of our cohort (n=13) to find out other possibly pathogenic variants that might support its involvement in SMS-like onset. Surprisingly, a second male patient (SMS2) with c.*182A>C genetic transversion on exon 12 (3'UTR of *ZDHHC15*) emerged (Fig.22).

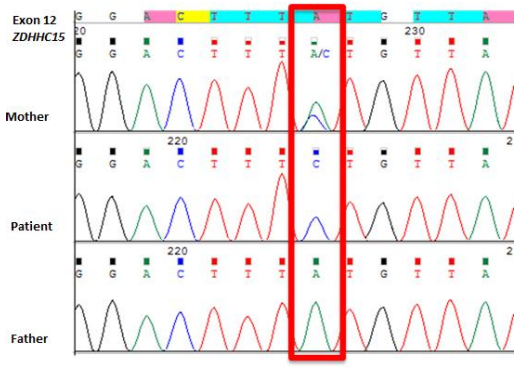

Fig.22- Electropherogram of patient SMS2 with *ZDHHC15* 3'UTR transversion and his parents.

Even SMS2 mutation is rare, has been never reported among the databases analyzed (Ensembl, dbSNP, HGMD, ExAC browser) and maternally inherited. SMS2 shows together with cognitive developmental delays the following SMS clinical features: short stature, squared-shaped face and slight prognatia, brachydacthyly, behavioural issues and sleep deficiencies. As resulted in SMS1 patient, SMS known molecular defects were ruled out and RT-qPCR on SMS2 blood derived RNA to test *RAI1* transcript levels resulted similar to ten healthy controls (Fig.23).

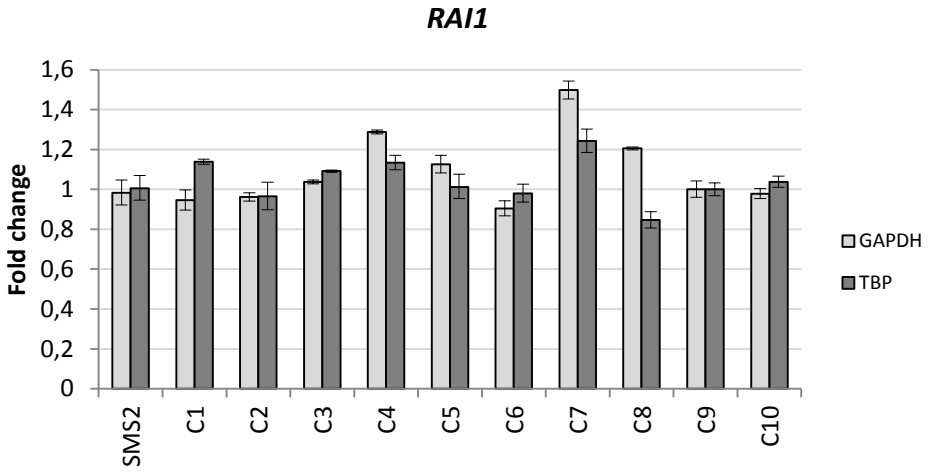

Fig.23- RT-qPCR of *RAI1* expression on SMS2 and ten healthy controls (C1-C10), C1-C5 are female controls, C6-C10 are male controls. RT-qPCR was performed twice using two different housekeeping genes, *TBP* and *GAPDH*.

Since the transversion detected in SMS2 is on 3'UTR, which has a role in translation efficiency, location, and stability of mRNAs, we postulated that the variant might have an effect on *ZDHHC15* transcript regulation or translation. To assess this potential effect on transcript we performed RT-qPCR analyses on blood mRNA of SMS2 and ten healthy male controls (Fig.24).

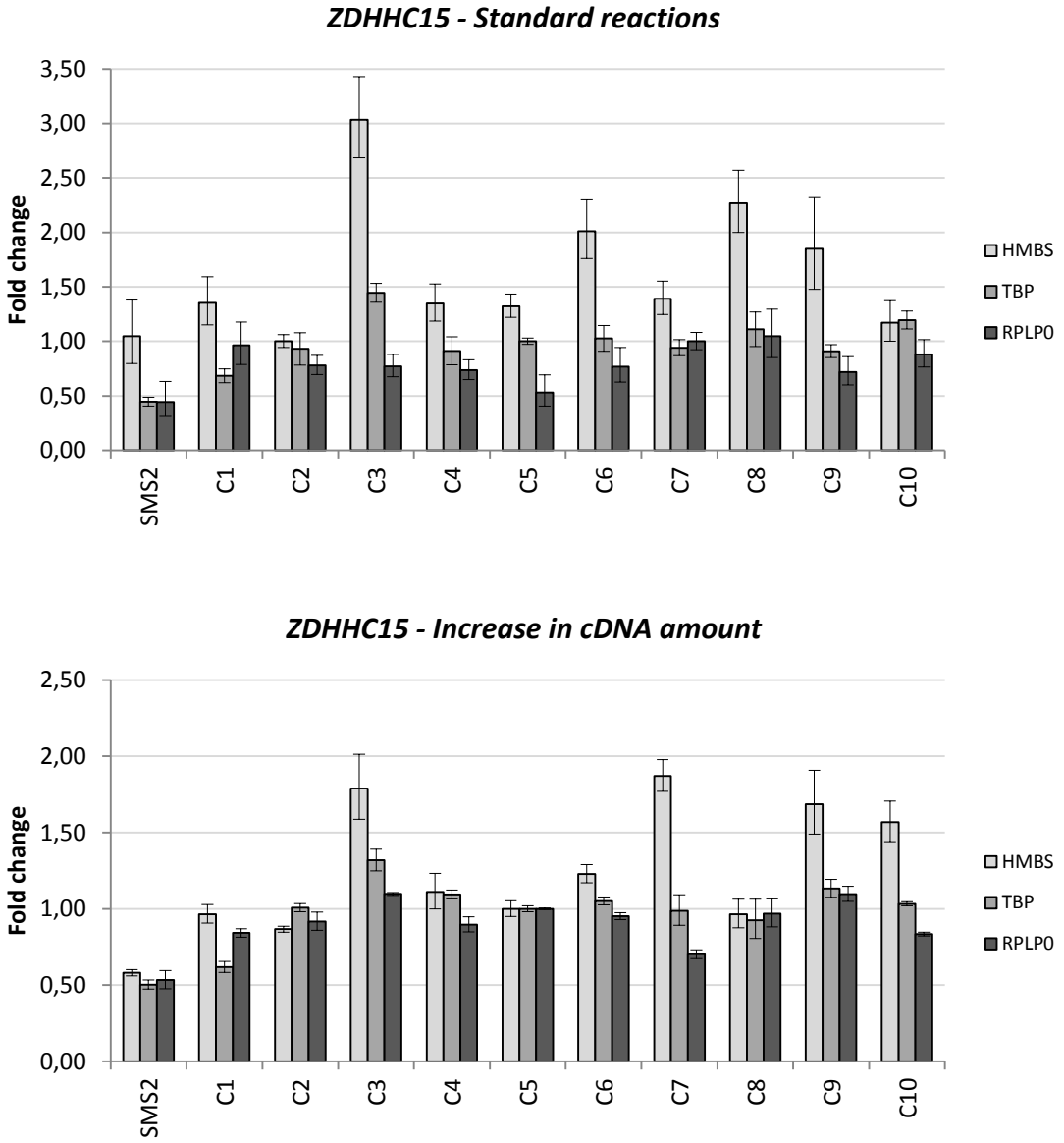

Fig.24- RT-qPCRs of *ZDHHC15* expression on SMS2 with *ZDHHC15* 3'UTR transversion and ten healthy male controls (C1-C10). Standard reactions are shown on the upper side, reactions with increased amount of cDNA on the bottom side. In both reaction series were used three different housekeeping genes, i.e. *HMBS*, *TBP* and *RPLP0*.

RT-qPCR analyses were performed using different housekeeping genes (*HMBS*, *TBP* and *RPLP0*) initially according to standard amount of cDNA per reaction (12.5 ng). Normalized on *HMBS* and *RPLP0*, *ZDHHC15* levels of SMS2 resulted similar to ten healthy male controls (Fig.24, upper side), whereas normalized on *TBP* (Fig.24, upper side) SMS2 *ZDHHC15* mRNA expression

seemed slight downregulated. Notably *ZDHHC15* mRNA resulted variably and poorly expressed in blood tissue, with high Ct values, thus affecting reproducibility and reliability of RT-qPCR data. To overcome this issue and clarify the suspicion of *ZDHHC15* downregulation, the same RT-qPCR were replicated using an higher amount of cDNA (140 ng per reaction) for both SMS2 and controls. The analyses supported the initial suspicion even if data were not statistically significant (Fig.24, bottom side).

To corroborate RT-qPCR data an absolute *ZDHHC15* quantitation on SMS1 and SMS2 blood extracted RNA was performed by digital PCR. SMS1 patient significant *ZDHHC15* downregulation was consistent with RT-qPCR data, while for SMS2 the suspicion of a slight *ZDHHC15* was not clarified. Indeed SMS2 cDNA *ZDHHC15* copies/microliter resulted within the control variability range, even if with the lowest value (Fig.25).

Sample	Copies/ microliter	CI copies/ microliter	Precision
SMS1	12,598	10.741 -- 14.777	17,29%
SMS2	29,936	26.974 -- 33.223	10,98%
C1	55,353	51.165 -- 59.885	8,19%
C2	48,566	44.794 -- 52.656	8,42%
C3	66,734	62.223 -- 71.572	7,25%
C4	35,546	32.497 -- 38.88	9,38%
C5	34,561	31.408 -- 38.03	10,04%
C6	72,495	67.855 -- 77.453	6,84%
C7	52,606	48.703 -- 56.821	8,01%
C8	41,873	38.463 -- 45.584	8,86%
C9	59,785	55.611 -- 64.273	7,51%
C10	42,676	39.163 -- 46.504	8,97%

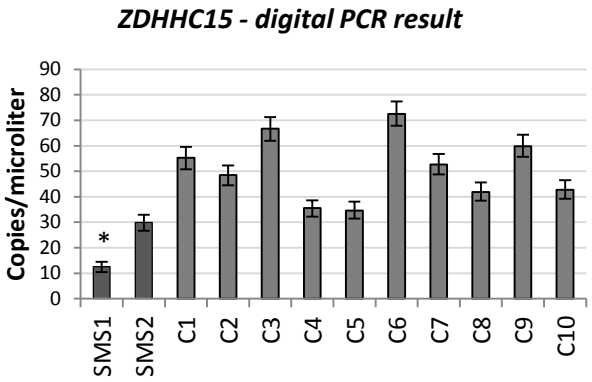

Fig.25- Digital PCR results. SMS1 and SMS2 *ZDHHC15* copies/microliter and ten healthy male controls (C1-C10) are shown. Student T test, *P<0.01.

4.3.3_miRNAs and Luciferase assay: does 3'UTR variant have an effect?

Since 3'UTR region is known to play a pivotal role in stability and regulation of mRNAs, we investigated whether specific miRNAs predicted to bind *ZDHHC15* 3'UTR might potentially modulate *ZDHHC15* expression and in particular, we studied if the c.*182A>C variant could change or introduce new miRNA sites in *ZDHHC15* 3'UTR. To get a list of miRNAs putatively interacting with wild type *ZDHHC15* 3'UTR we used different bioinformatic tools such as, miRdb, DIANA, miRanda, and TargetScan. These prediction softwares are based on complementarity but use different algorithms leading to different predictions. For this reason the resulting miRNAs list was not consistent switching from one tool to the other. Therefore we

chose the miRNAs recurrent in at least two softwares, such as hsa-miR-142-5p and hsa-miR-5590-3p (Tab.6). TargetScan revealed a specific pairing between seed sequence of these two miRNAs and the wild type *ZDHHC15* 3'UTR where our transversion occurred, thus further corroborating the *in silico* predictions (Fig.26).

Tab.6. *In silico* predictions of miRNa binding site in the ZDHHC15 3'UTR sequence spanning the c.*182A>C (miRDB, Diana, miRanda, TargetScan).

miRNA	miRDB	Diana	miRanda	TargetScan
hsa-miR-142-5p	no	yes	yes	yes
hsa-miR-5590-3p	no	yes	no	yes

Fig.26-TargetScan output, pairing between hsa-miR-142-5p, hsa-miR-5590-3p and wild type *ZDHHC15* 3'UTR. Red asterisk highlights where c.*182A>C occurred.

To search for miRNAs putatively interacting with mutated *ZDHHC15* 3'UTR (c.*182A>C) we used miRdb custom and FindTar3 softwares. The list of miRNAs emerged from these two softwares resulted not consistent between each other and therefore we decided to use a third tool, RNAhybrid whose predictions are based on thermodynamic and statistical modeling. FindTar3 predictions resulted validated by RNAhybrid and we chose the three miRNAs, hsa-miR-922, hsa-miR-191-5p and hsa-miR-4797-5p, with the seed region perfectly paired to the first five nucleotides of *ZDHHC15* 3'UTR mutated site sequence (Fig.27).

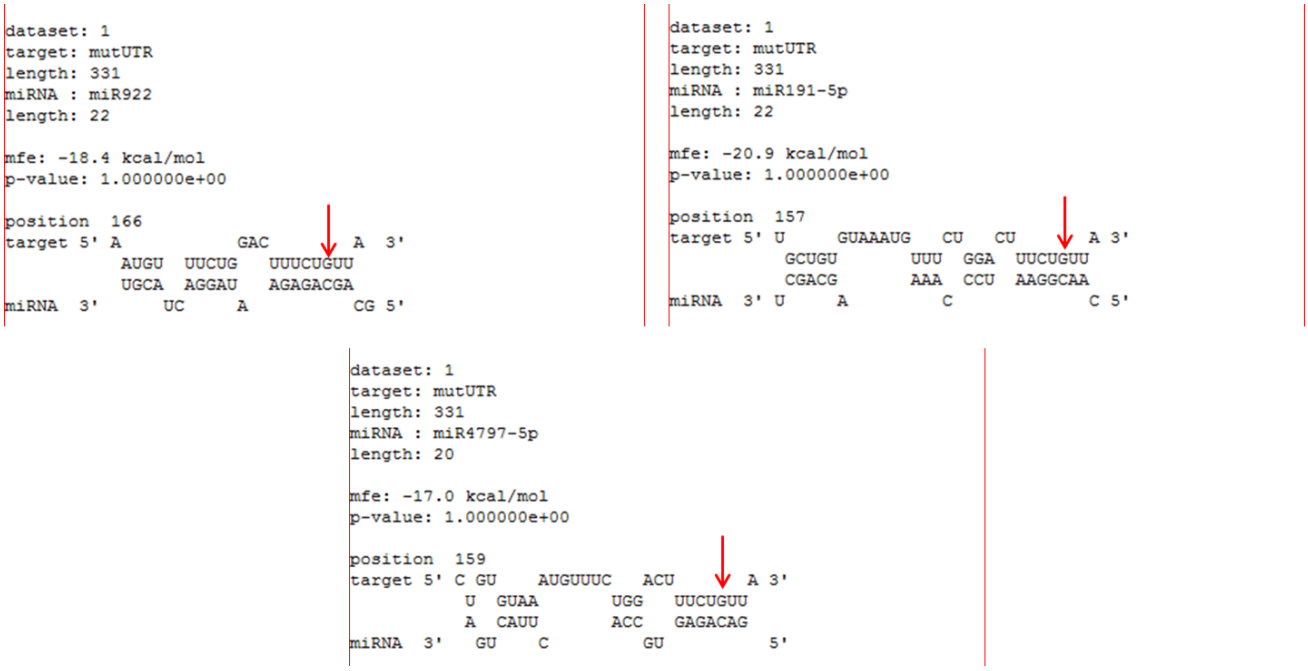

Fig.27- RNA hybrid output for hsa-miR-922 (miR922), hsa-miR-191-5p (miR191-5p) and hsa-miR-4797-5p (miR4797-5p) and the mutant 3'UTR sequence. Red arrow highlights the c.*182A>C variant.

The expression pattern of the two miRNAs putatively interacting with wild type *ZDHHC15* 3'UTR and of the three miRNAs putatively interacting with mutated *ZDHHC15* 3'UTR was checked on tissue expression Atlas (https://www.ebi.ac.uk/; https://www.ncbi.nlm.nih.gov/geo/). Interestingly, we found that hsa-miR-142-5p is highly expressed in brain while hsa-miR-922, hsa-miR-191-5p and hsa-miR-4797-5p are variably expressed in frontal cortex and cerebellum.

To validate the predicted miRNAs *in vitro* we tested their inhibitory effect on *ZDHHC15* 3'UTR sequence (321bp) using luciferase assay. We co-transfected HEK293T cell line with a luciferase reporter plasmid containing wild type or mutated *ZDHHC15* 3'UTR fragments (321bp) and each of the selected miRNAs (hsa-miR-142-5p, hsa-miR-5590-3p, hsa-miR-922, hsa-miR-191-5p and hsa-miR-4797-5p).

According to *in silico* predictions, miR-5590-3p significantly downregulated luciferase transcripts containing wild type 3'UTR sequence. In particular a significant and specific downregulation of wild type transcript to 0.80 fold was observed compared to negative control miRNA (Fig.28A). Regarding miR-142-5p, it downregulated significantly both wild type and mutated luciferase transcripts to respectively 0.84 and 0.91 fold (Fig.28B).

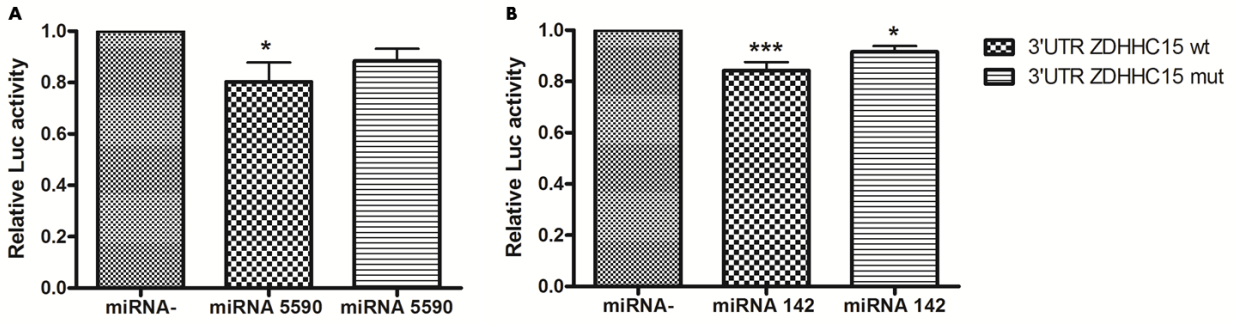

Fig.28- Relative luciferase activity of wild type (*ZDHHC15* 3'UTR) and mutant (*ZDHHC15* 3'UTR) firefly constructs in HEK293T cells transfected with negative control miRNA (miRNA-), miR-142-5p or miR-5590-3p. Normalized firefly luciferase activity was represented relative to control miRNA transfected cells. A) hsa-miR-5590-3p bar graph; B) hsa-miR-142-5p bar graph. Mean ± SEM; n=8; One-Way Anova with Tukey post-hoc Test *P<0.05 ; ***P<0.001.

Regarding the set of miRNAs putatively binding the mutated 3'UTR sequence we observed that luciferase values were significantly decreased for mutated *ZDHHC15* 3'UTR reporter construct only with transfection of miR-4797-5p (Fig.29). Specifically, miR-4797-5p downregulated to 0.78 fold the luciferase activity of the construct containing the mutant 3'UTR sequence (Fig.29A), while no significant change in luciferase activity was observed neither using miR-922 (Fig.29B) nor using miR-191-5p in the assay (Fig.29C).

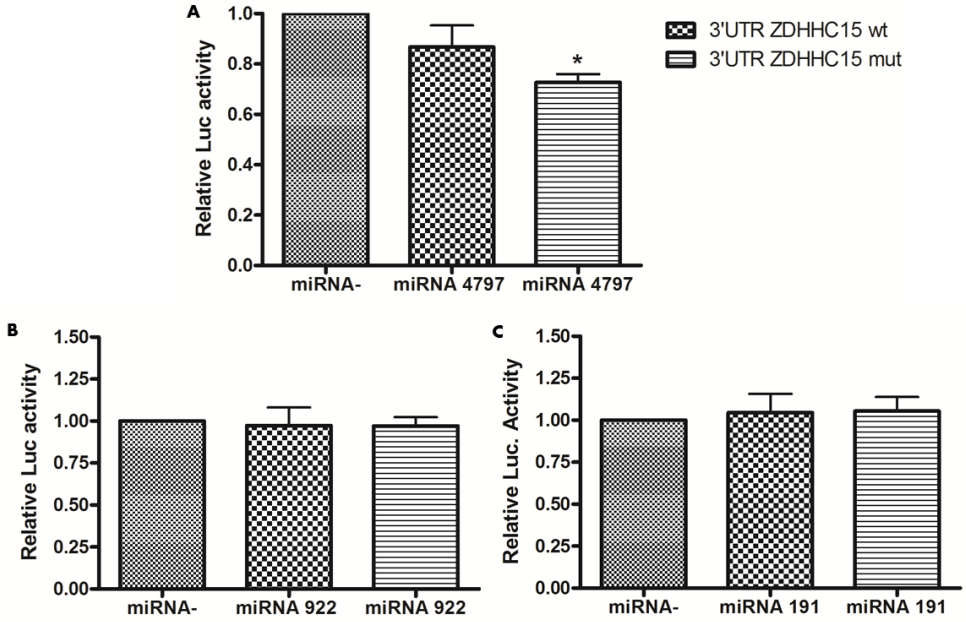

Fig.29- Relative luciferase activity of wild type (*ZDHHC15* 3'UTR) and mutant (*ZDHHC15* 3'UTR) firefly constructs in HEK293T cells transfected with negative control miRNA (miRNA-), miR-4797-5p, miR-922 and miR-191-5p. Normalized firefly luciferase activity was represented relative to control miRNA transfected cells. A) hsa-miR-4797-5p; B) hsa-miR-922 bar graph; C) hsa-miR-191-5p bar graph. Mean ± SEM; n=3; One-Way Anova with Tukey post-hoc Test *P<0.05.

In conclusion among the miRNAs emerged from prediction softwares only hsa-miR-5590-3p and hsa-miR-4797-5p resulted validated *in vitro* by luciferase assays. miR-5590-3p specifically downregulated the luciferase activity of firefly construct containing wild type *ZDHHC15* 3'UTR (Fig.28A), while miR-4797-5p specifically downregulated the luciferase activity of firefly construct containing mutated *ZDHHC15* 3'UTR (Fig.29A). Thus we can speculate that c.*182A>C transversion found in SMS2 patient may have an effect by creating a new binding site for hsa-miR-4797-5p and in parallel by abolishing hsa-miR-5590-3p target site.

4.3.4_Analysis of ZDHHC15 protein content in whole blood

Due to the 3'UTR role in translational control, we investigated ZDHHC15 protein levels in the available whole blood cellular extracts from SMS2 patient, four healthy controls and a positive control cell line (such as the human neuroblastoma SK-N-BE cells). We set up protein extraction and performed Western Blot analysis using anti-ZDHHC15 commercial antibody. We failed to detect any specific ZDHHC15 band although all samples were positive for GAPDH marker. The company later confirmed that their antibody was ineffective and other commercial antibodies were not available for further testing. Thus we were unable to define c.*182A>C 3'UTR transversion effect at protein level.

4.4_Prediction of putative palmitoylation sites in RAI1 and other proteins related to circadian rhythms

As mentioned before, *ZDHHC15* encodes for a palmitoyl-transferase (PAT), a family of enzymes that catalyze the transfer of a palmitate on cysteine residue of its target protein, by thioester bond. Palmitoylation is a reversible post-translational modification that modulates protein trafficking and stability (Mitchell et al 2010). Actually ZDHHC15 specific substrates are not known, but *zdhhc15b*, the zebrafish horthologue of human *ZDHHC15*, was shown to be crucial for dopaminergic neuron development (Wang et al 2015). Since both *zdhhc15b* and *RAI1* play a role in neurodevelopment (Bi et al 2005; Tahir et al 2014; Wang et al 2015; Huang et al 2016), we wondered whether RAI1 would have any palmitoylation sites further supporting a possible functional correlation between RAI1 and ZDHHC15 proteins. Despite the lack of a common

canonical consensus sequence for palmitoylation (el-Husseini Aelm, Bredt 2002; Linder, Deschens 2003), CSS-Palm software which allows *in silico* predictions of potentially palmitoylated peptide sites was interrogated (Zhou et al 2006). Basically the higher the score of a peptide sequence predicted by CSS-Palm is, the higher confidently we may assert that this peptide may be palmitoylated. *In silico* analysis by CSS palm software revealed putative palmitoylation sites in RAI1 aminoacidic sequence (Tab.7).

Tab.7- RAI1 predicted sites CSS-Palm output.

ID	Position	Peptide	Score	Cutoff	Type
RAI1	8	MQSFRERCGFHGKQQ	1.644	1.396	S-Palmitoylation: Cluster C
	1516	QPPEGRPCQPQTRAQ	1.671	1.396	S-Palmitoylation: Cluster C
	1687	LSTSCLVCCLCQNPA	2.907	1.396	S-Palmitoylation: Cluster C
	1688	STSCLVCCLCQNPAN	1.426	1.396	S-Palmitoylation: Cluster C
	1783	LSRRLQSCYCCDGRE	1.916	1.396	S-Palmitoylation: Cluster C
	1785	RRLQSCYCCDGREDG	3.09	3.076	S-Palmitoylation: Cluster B
	1869	EAGATIGCCHKGCLH	1.592	1.396	S-Palmitoylation: Cluster C

In particular, RAI1 is predicted to have seven palmitoylation sites mostly located within the C-terminal domain (Fig.30) and two of them at aminoacidic positions 1687 and 1785 having an high clustering score close to 3.0 (Tab.7).

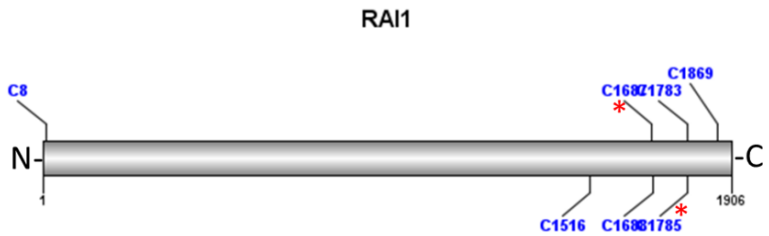

Fig.30- RAI1 protein with putative palmitoylation sites. Cysteine position is labeled in blue, red asterisks highlight cysteines with highest prediction score.

To further corroborate the hypothesis that ZDHHC15 may play a role in the same biological pathways of RAI1, *in silico* prediction analysis by CSS-Palm software was extended to MBD5 and HDAC4 proteins which were previously shown to be related to *RAI1* gene expression (Williams et al 2010 b; Mullegama et al 2015 a). Both MBD5 and HDAC4 resulted putatively palmitoylated, specifically HDAC4 displayed a clustering score >3 for the cysteine 932 (Tab.8). Due to involvement of RAI1 in circadian gene control (William et al 2012) and the clinical relevance of circadian rhythms alterations in Smith Magenis Syndrome, an eventual link between ZDHHC15 and circadian gene was postulated. Thus we extend our analysis with CSS-Palm software to 16 main circadian proteins (BMAL1, BMAL2, CLOCK, CRY1, CRY2, CSNK1D,

CSNK1E, FBXL3, NR1D1, NR1D2, PER1, PER2, PER3, RORA, RORB, RORC). According to *in silico* predictions 9 of them (BMAL1, BMAL2, CLOCK, FBXL3, PER1, PER2, PER3, RORA and RORB) are supposed to be palmitoylated (Tab.8). Notably, 5 out of 9 show up to three palmitoylation sites (BMAL1, PER2, PER3, RORA and RORB) (Tab.8).

In line with the observation that RAI1 may control *BDNF* gene expression (Bi et al 2005) and that RAI1 and its putative interactor SIRT1 seem to regulate neuronal plasticity and circadian rhythms genes (Garay et al 2016), we checked whether SIRT1 and BDNF might also be palmitoylated. SIRT1 amminoacidic sequence resulted potentially palmitoylated in two sites, with a clustering score >3.5 at cysteine 371 (Tab.8) while BDNF did not have any predicted palmitoylation site (Tab.8).

Tab. 8- RAI1 regulators and circadian proteins palmitoylation sites

ID	Position	Peptide	Score	Cutoff	Type
BDNF	No site predicted				
BMAL1	35	LGTSGVDCNRKRKGS	2.123	1.396	S-Palmitoylation: Cluster C
	240	TPGPSRLCSGARRSF	3.236	3.076	S-Palmitoylation: Cluster B
BMAL2	20	VLREENQCIAPVVSS	2.45	1.983	S-Palmitoylation: Cluster A
CLOCK	7	*MLFTVSCSKMSSIV	1.999	1.396	S-Palmitoylation: Cluster C
CRY1	No site predicted				
CRY2	No site predicted				
CSNK1D	No site predicted				
CSNK1E	No site predicted				
FBXL3	63	RAHASQVCRNWNQVF	3.899	3.076	S-Palmitoylation: Cluster B
HDAC4	982	GHDLTAICDASEACV	3.547	3.076	S-Palmitoylation: Cluster B
MBD5	315	PVMKKPMCNFSTNME	1.44	1.396	S-Palmitoylation: Cluster C
NR1D1	No site predicted				
NR1D2	No site predicted				
PER1	550	PVTFQQICKDVHLVK	3.275	3.076	S-Palmitoylation: Cluster B
PER2	962	IPRQPCACPATRATP	1.649	1.396	S-Palmitoylation: Cluster C
	1084	LGSGSLGCDASPSGA	2.314	1.396	S-Palmitoylation: Cluster C
PER3	204	RAAARYECAPVKPFF	3.13	3.076	S-Palmitoylation: Cluster B
	778	AHQNAQPCCPSAASS	3.923	3.076	S-Palmitoylation: Cluster B
	876	LSPSFLPCPFLGATA	2.648	1.396	S-Palmitoylation: Cluster C
RORA	25	PWSIMGHCLRTGQAR	1.419	1.396	S-Palmitoylation: Cluster C
	73	AFVLTGVCCSWRQNG	1.777	1.396	S-Palmitoylation: Cluster C
RORB	10	AQIEVIPCKICGDKS	2.183	1.396	S-Palmitoylation: Cluster C
	13	EVIPCKICGDKSSGI	1.799	1.396	S-Palmitoylation: Cluster C
	454	KELFNPDCATGCK**	4.792	3.076	S-Palmitoylation: Cluster B
RORC	No site predicted				
SIRT1	67	VPAAARGCPGAAAAA	1.426	1.396	S-Palmitoylation: Cluster C
	371	GSFATASCLICKYKV	3.586	3.076	S-Palmitoylation: Cluster B

4.5_Effect of *ZDHHC15* and *RAI1* knockdown on expression of circadian rhythm-related genes

In order to support *ZDHHC15* involvement in SMS manifestation, specifically in circadian rhythm, we set up gene silencing experiments in human BE (2)-M17 neuroblastoma cells to check whether *RAI1* and *ZDHHC15* knockdown would raise the same effect. Even though *RAI1* involvement in circadian rhythm-related genes has been already reported in a previous publication (Williams et al 2012) we wanted to repeat the silencing experiments using a neuronal cell line expressing both *RAI1* and *ZDHHC15*.

We obtained a gene silencing efficiency of 42% and 62% for *RAI1* (Fig.31A) and *ZDHHC15* (Fig.31B), respectively, compared to negative control siRNA silenced cells. To reveal eventual expression change in genes directly related to *RAI1* (*MBD5*, *HDAC4*), possibly interacting with RAI1 at chromatin level (*SIRT1*) (Garay et al 2016), and main circadian genes (*BMAL1, BMAL2, CLOCK, CRY1, CRY2, CSNK1D, CSNK1E, FBXL3, NR1D1, NR1D2, PER1, PER2, PER3, RORA, RORB, RORC*), we performed RT-qPCR assay.

We first evaluated whether knockdown of *RAI1* gene would have any effect on the expression level of *ZDHHC15* and *vice versa*. *RAI1* silenced samples did not show any change in *ZDHHC15* gene expression levels (Fig.31C). On the contrary a marked, even if not significant, upregulation of *RAI1* expression levels was observed in *ZDHHC15* silenced samples (Fig.31D). We should probably increase the number of experiments to reach statistical significance.

The gene expression level of *RAI1* putative regulators *HDAC4* and *MBD5* showed no significant changes neither in *RAI1* silenced (Fig. 31C) nor in *ZDHHC15* silenced cells (Fig. 31D). In *ZDHHC15* knocked down cells an increase in *HDAC4*, *MBD5* and *SIRT1* mRNA content was observed even though without statistical significance (Fig. 31D).

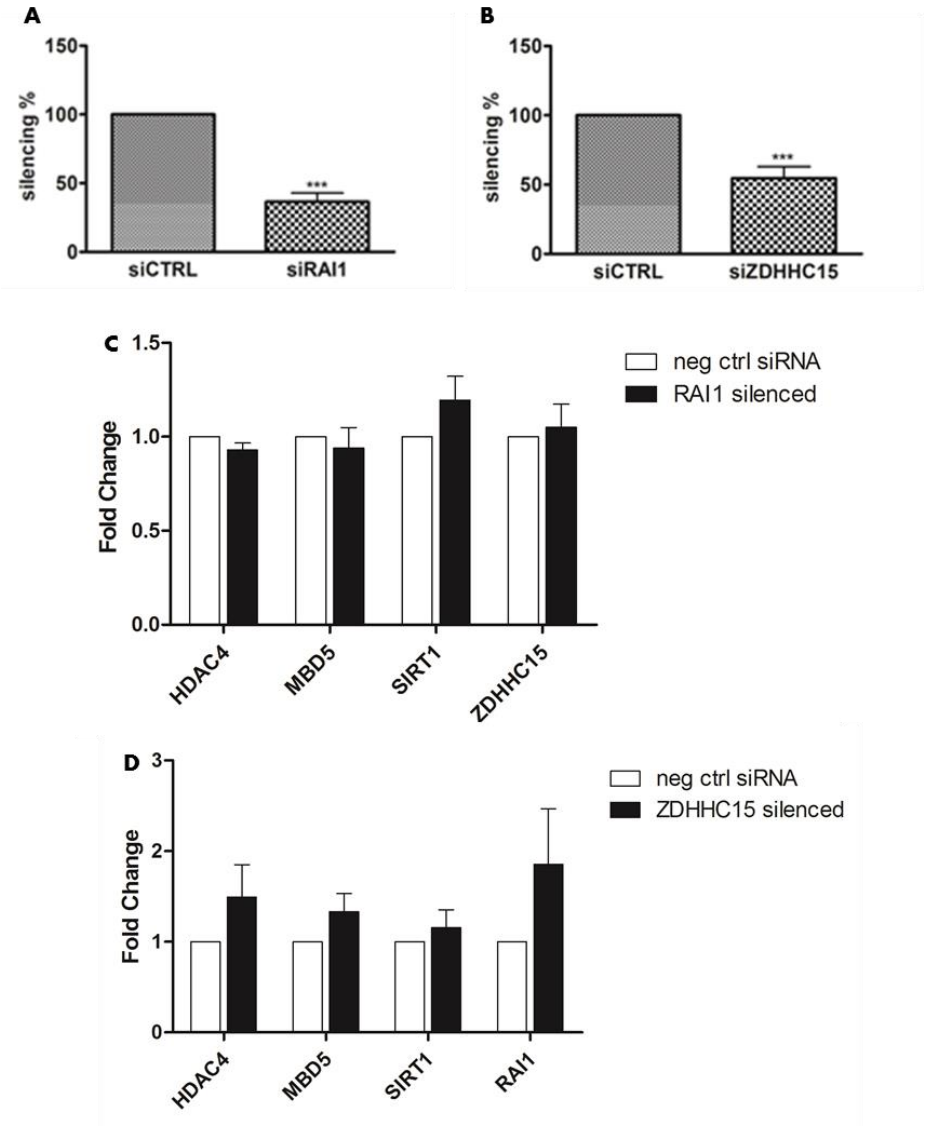

Fig.31- Gene silencing experiments and quantitative analysis of gene expression changes. A) *RAI1* B) *ZDHHC15* were knocked down in BE(2)-M17 cells using a stealth miRNA with medium GC content as negative control (siCTRL) and their gene silencing efficiency was evaluated by RT-qPCR assay (Mean ± SEM; n=4; One tailed Student T-test ***P<0.0001). Fold change values of putatively *RAI1* regulators *HDAC4* and *MBD5*, interactor *SIRT1* and "indirect modulator" *ZDHHC15* in C) *RAI1* silenced and in D) *ZDHHC15* silenced cells are indicated (black bar) compared to negative control siRNA (white bar).

Among the circadian rhythms genes tested (*CLOCK*, *BMAL1*, *PER3, BMAL2*, *RORC*, *FBXL3*, *CSNK1D*, *CSNK1E, NR1D1*, *NR1D2*, *PER1*, *PER2, CRY1*, *CRY2*) a statistically significant dysregulation of *PER3*, *RORC*, *CSNK1D*, *CSNK1E, NR1D1*, *PER2* and *CRY1* gene expression levels in *RAI1* silenced cells emerged by RT-qPCR analysis (Fig.32). *PER3*, *CSNK1D*, *CSNK1E*, *PER2* and *CRY1* mRNA content resulted downregulated, whereas *RORC* and *NR1D1* gene expression levels resulted upregulated in *RAI1* silenced samples compared to negative control siRNA (Fig.32). Notably, *RORC* gene expression increased by 3.25 fold compared to negative control

siRNA (Fig.32). A trend to increase in *CRY2* gene expression was observed even if not statistical significant (Fig.32).

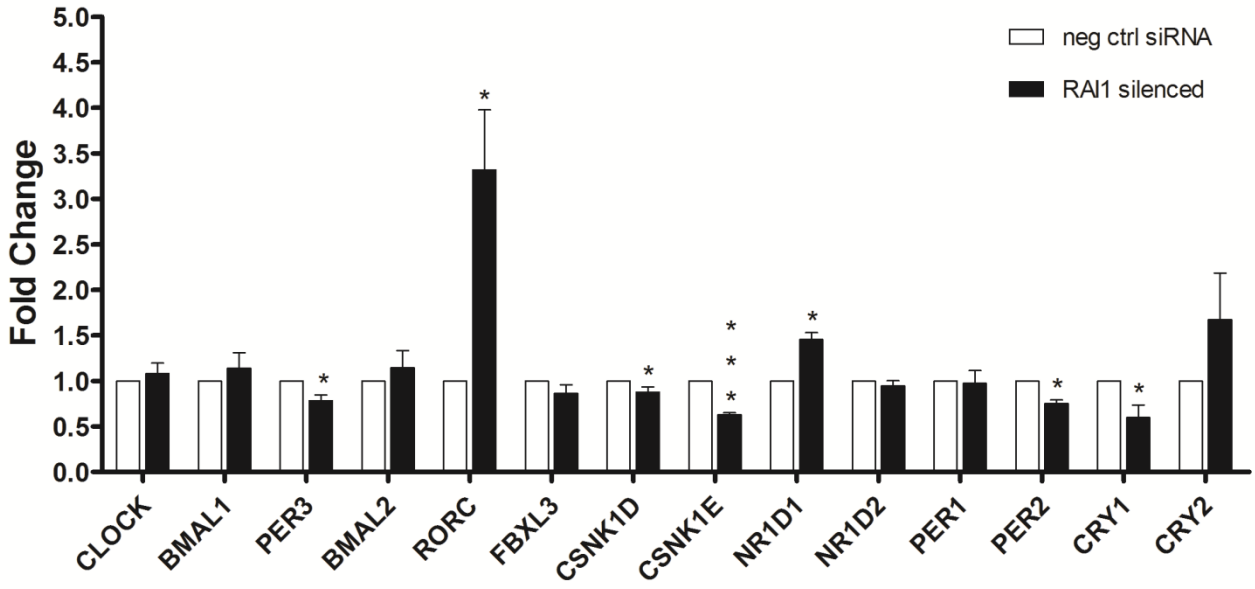

Fig.32- Quantitative analysis of circadian rhythm genes expression level (fold change) in *RAI* silenced samples. Negative control siRNA (white bar) vs *RAI* silenced samples (black bar). Mean ± SEM; n=4; One tailed Student T-test *P<0.05 and ***P< 0.001.

When we analyzed the expression of the circadian genes in *ZDHHC15* knocked down cells 6 (*BMAL1*, *PER3*, *BMAL2*, *RORC*, *FBXL3*, *NR1D2*) out the 14 circadian genes tested analyzed emerged as dysregulated by RT-qPCR assay (Fig.33). In particular mRNA levels of *BMAL1*, *RORC* and *NR1D2* resulted upregulated compared to negative control siRNA samples with *RORC* and *NR1D2* showing an increase to ~ 2 folds (Fig.33). Whereas the gene expression levels of *PER3*, *BMAL2* and *FBXL3* resulted downregulated and specifically *BMAL2* level decreased by ~ 0.5 fold (Fig.33). Even though not statistically significant a trend to be upregulated was observed for *CSNK1D*, *CSNK1E*, *NR1D1* and *CRY2* genes in *ZDHHC15* silenced samples compared to negative control siRNA samples (Fig.33).

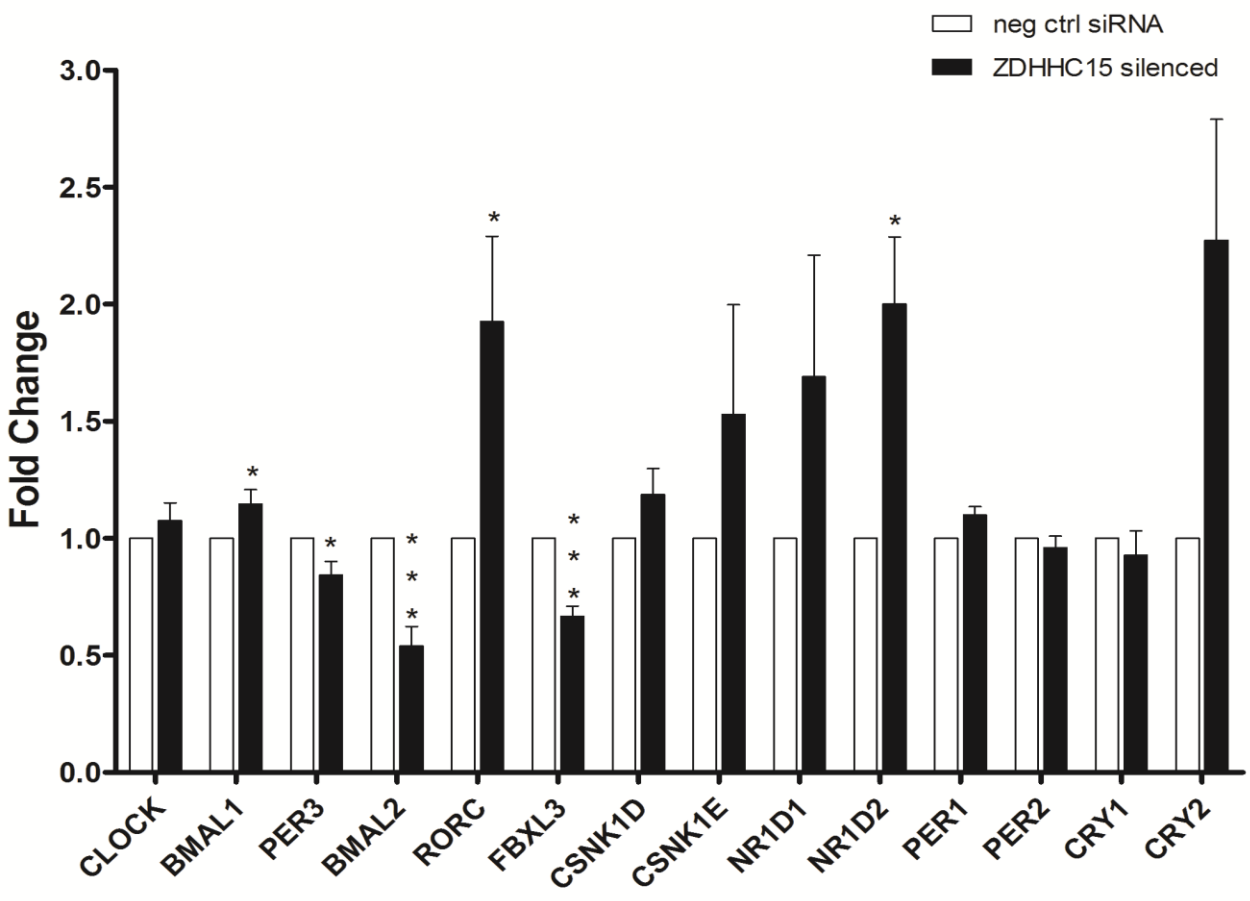

Fig.33- Quantitative analysis of circadian rhythm genes expression levels (fold change) in *ZDHHC15* silenced samples. Negative control siRNA (white bar) vs *ZDHHC15* silenced samples (black bar). Mean ± SEM; n=4; One tailed Student T-test *P<0.05 and ***P< 0.001.

In conclusion among 14 main circadian genes tested *PER3* and *RORC* showed similar gene expression change in both *RAI1* and *ZDHHC15* silenced cells, specifically *PER3* resulted downregulated while *RORC* markedly upregulated.

Notably, even if not statistically significant in *ZDHHC15* silenced samples, *NR1D1* and *CRY2* showed a similar upregulation of their expression levels in both *RAI1* and *ZDHHC15* knocked down cells. On the other hand, *RAI1* silenced cells revealed a trend opposite to *ZDHHC15* silenced ones regarding *CSNK1D* and *CSNK1E* gene expression levels, which were significant only in *RAI1* knocked down cells. It would be worthwhile to increase the number of experiments to try to improve statistical significance of these data. We failed to analyze *BDNF* gene expression levels because its expression in BE(2)-M17 *in vitro* system was too low (Ct>32).

DISCUSSION

Smith Magenis Syndrome (SMS, OMIM#182290) is a dominant disorder, with an estimated prevalence of 1:15000-25000, mainly resulting from haploinsufficiency of *RAI1* gene due to either 17p11.2 deletion or *RAI1* mutation.

Despite *RAI1* is recognized as the disease-causing gene just 50% of patients with a suspicion of SMS have SMS classical genetic defects, thus it is likely that other loci, with a role in the same RAI1 functional pathway or regulating directly *RAI1* transcription, might be involved in SMS aetiology and eventually explain SMS similar phenotypes. Indeed recent array CGH studies on SMS-like cohort identified patients with two SMS overlapping syndromes, 2q23.1 deletion syndrome (OMIM#156200) and Brachydactly Mental Retardation syndrome (BDMR, OMIM#600430), due to *MBD5* and *HDAC4* haploinsufficiency respectively (Williams et al 2010 a). *MBD5* and *HDAC4* are two chromatin remodelers crucial for brain plasticity (Talkowski et al 2011; Sando et al 2012); interestingly patients with *MBD5* or *HDAC4* haploinsufficiency display *RAI1* downregulation, according to their SMS overlapping phenotypes (Williams et al 2010 b; Mullegama et al 2015 a). Genome-wide approach on a cohort of patients with a clear SMS phenotype but lacking 17p11.2 microdeletion or *RAI1* molecular defects is useful to unravel RAI1 functional pathways. Indeed, even if *RAI1* is recognized as the disease-causing gene its detailed role in different molecular pathways remains elusive. Several animal models support RAI1 crucial contribution to brain development and plasticity, by interacting at chromatin promoter and enhancer regions, but compelling evidences on RAI1 regulators, interactors and targets are still missing.

Therefore a previously selected cohort of 40 patients analyzed according to diagnostic guidelines and negative to 17p11.2 microdeletion or *RAI1* mutations, thus referred as “Smith Magenis like patients” (SMS-like), was screened with high resolution array CGH analysis searching for rare CNVs with a putative pathogenic effect because disrupting dosage-sensitive genes implicated in the onset of SMS phenotype. The present analysis revealed to be effective in identifying candidate genes possibly implicated in RAI1 functional pathway. Indeed, among SMS-like patients a rare 54 kb deletion on Xq13.3 identified in a male patient (SMS1) and maternally inherited was considered to be of particular interest because, even if the deletion does not involve any genes, maps 29 kb far from the 5’UTR of *ZDHHC15* (Zinc Finger DHHC domain-containing protein 15), a gene previously found not expressed in a patient with a nonsyndromic X-linked intellectual disability (XLID) (Mansouri et al 2005). Notably, in SMS1, *ZDHHC15* transcript resulted statistically downregulated according to RT-qPCR analyses: in our

hypothesis, the Xq13.3 deletion, removing a conserved insulator element with CTCF binding site, might have perturbed the chromatin status by a position effect, thus leading to heterochromatinization of the adjacent region and a subsequent gene downregulation (Fig.34).

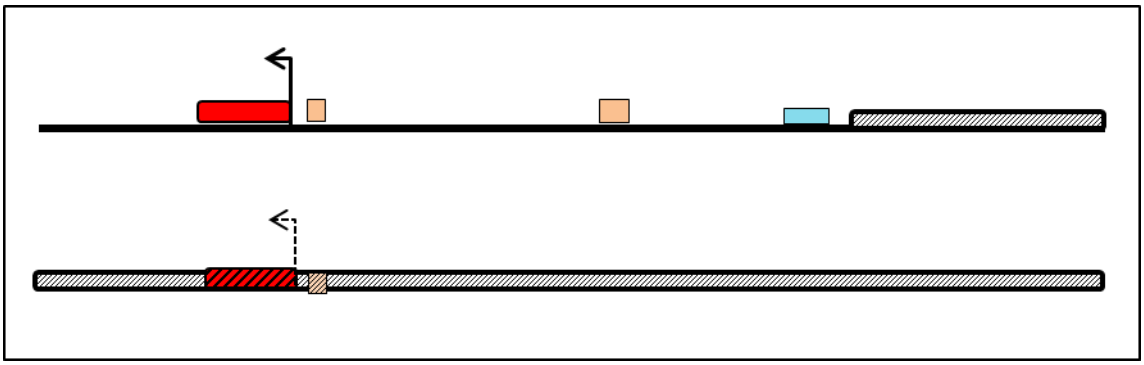

Fig.34- Model of position effect hypothesis. Variation of chromatin conformation due to the insulator loss. Genomic deletion including insulator (blue blocks) might switch an euchromatic gene region (upper side of panel) to heterochromatic state (bottom side of panel) alteration causing silencing/downregulation of the flanking gene/nearby gene. Promoter and enhancer are shown respectively as red and yellow blocks, heterochromatic status by grey pattern thick line.

As we posited a long range heterochromatinization it might be helpful to investigate the expression levels of *ZDHHC15* neighboring genes and eventually look at methylation status of their promoters to further sustain our hypothesis.

This hypothesis is also confirmed by an *in silico* analysis searching for Topologically Associated Domains (TADs) in Xq13.3 deleted region. Recent studies on chromatin three-dimensional nuclear organization of mammalian genomes revealed the presence of genomic regions called TADs (Lupianez et al 2015) that if disrupted (e.g. due to genomic structural variants) could affect the expression of nearby genes often leading to diseases (Lupianez et al 2016). As shown in Fig.35 the Xq13.3 deletion identified in SMS1 seems to disrupt the boundaries of two/three adjacent TADs. Assuming that the TAD in which *ZDHHC15* localizes is actively transcribed and that the distal one is inactively transcribed, the lack of these boundaries might have altered the chromatin status of the active TAD, thus supporting our RT-qPCR data and the assumption of a long range heterochromatinization.

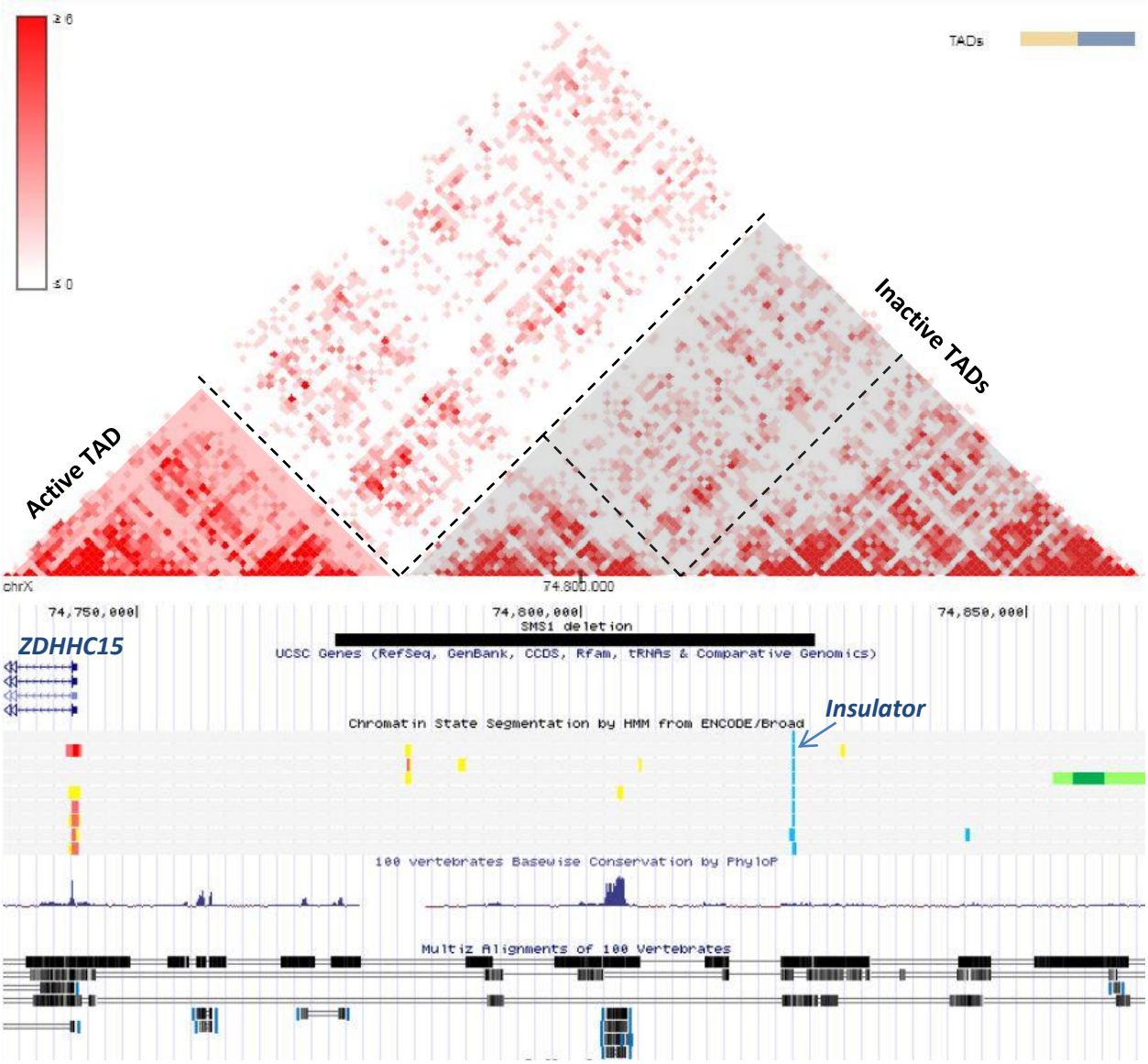

Fig.35- Hi-C data visualization on UCSC genome browser. GM12878 cell line with 1 kb resolution was selected. TADs are visualized by dotted lines. SMS1 deletion with the insulator element predicted (in light blue) is shown upstream 5'UTR of *ZDHHC15* (http://promoter.bx.psu.edu/hi-c/view.php).

As previously mentioned Mansouri et al. described in 2005 a female patient with a severe intellectual disability who carries a balanced reciprocal t(X;15)(q13.3;cen). The breakpoint at Xq13.3 is located within the first exon of *ZDHHC15* gene resulting in absence of any *ZDHHC15* transcripts due to an expected shewed X inactivation. Interestingly, although this patient and SMS1 share some clinical features (i.e. intellectual disability, hypotonia, speech delay and aggressive behavior), the phenotype of the female patient reported by Mansouri et al. is more

severe compared to SMS1 phenotype; this can be explained by her complete lack of *ZDHHC15* expression compared to the downregulation observed in SMS1.

Supporting the relationship between *ZDHHC15* and SMS-like manifestations, the subsequent Sanger sequencing performed on all male patients within SMS-like cohort, identified a second male patient (SMS2) with a rare variant (c.*182A>C) in 3'UTR regulatory region of *ZDHHC15* that was maternally inherited. Further quantitation of gene transcript levels in SMS2 revealed the possibility that a slight downregulation occurred. Even though Real Time data were not significant in the tissue analyzed it cannot be ruled out that a gene downregulation might be more evident in other tissues mainly involved in SMS pathophysiology.
Supporting the idea that the variant identified in SMS2 patient might raise an effect on *ZDHHC15* regulation, *in vitro* experiments using selected miRNAs for wild type and mutated sequence, revealed that SMS2 variant might effectively abolish a miRNA physiological binding site (hsa-miR-5590-3p downregulated only wild type 3'UTR of *ZDHHC15*) and create a new one (hsa-miR-4797-5p downregulated only mutated 3'UTR of *ZDHHC15*). Notably, hsa-miR-4797-5p expression is supposed to be variable in cerebellum and frontal cortex thus eventually explaining why on blood derived RNA *ZDHHC15* levels of SMS2 resulted just slightly downregulated.

Our focus on *ZDHHC15* as good candidate for SMS-like manifestation raised also according to its biological function. *ZDHHC15* encodes for palmitoyl-transferase 15 ubiquitously expressed, but highly expressed in brain. Palmitoyl-transferases (PATs) are a family of enzymes that catalyze the transfer of a palmitate on Cys residue of its target protein by thioester bond. The PAT gene family is deeply conserved across eukaryotes. Seven PAT genes are observed in yeast while tewnty-two in humans (Ohno et al 2006), encoding for their respective proteins, thus suggesting a fine tuned substrate specificity. In the past decade many advances were done to understand the palmitoylation and its relevance in brain (Fukata, Fukata 2010). Aberrant/defective palmitoylation has already been linked to Neuronal Lipofucinosis, Alzheimer Disease, mental retardation, Huntington Disease (Young et al 2012), thus giving compelling evidences of the critical role of PATs in neurodevelopmental and neuron survival processes. Recent palmitoylome studies on different cell types determined the palmitoylation contribution to several processes including cancer, immunity and synaptic function (Sanders et al 2015). This enrichment analyses revealed a potential role for palmitoylation at synapses since the 41% of

synaptic genes was found palmitoylated (Sanders et al 2015). About *ZDHHC15* specific function is only reported a study in which zebrafish *Zdhhc15b*, *ZDHHC15* human orthologue, was found to be crucial in diencephalic dopaminergic neurons differentiation (Wang et al 2015). Actually ZDHHC15 specific substrates are not known.

Based on ZDHHC15 role in post-translational modification and sustaining the idea that ZDHHC15 might modulate directly RAI1, thus being implicated in SMS/SMS-like onset, *in silico* analysis of RAI1 protein revealed two cysteine residues likely to be palmitoylated at C-terminal domain. Since this domain is crucial for RAI1 nuclear localization (Carmona Mora et al 2012), we can speculate that a defective palmitoylation might lead to RAI1 mislocalization, thus affecting RAI1 physiological/intracellular function and/or mimicking *RAI1* haploinsufficiency. If this idea is validated *in vitro*, it might explain why either *RAI1* either *ZDHHC15* downregulation results in similar neurological/neurobehavioural phenotypes. This eventual direct connection needs to be further addressed with other experimental procedures.

The hypothesis of an eventual indirect connection between ZDHHC15 and RAI1 was further supported by extending *in silico* palmitoylation predictions to *RAI1* putative regulators (HDAC4 and MBD5) and interactor SIRT1, that showed for each protein an high score for palmitoylation. Due to the relevance of sleep disturbance phenotype in SMS, also some of the circadian genes (n=9) are predicted to be palmitoylated, supporting ZDHHC15 indirect connection with RAI1 and circadian rhythms.

These results corroborated the hypothesis of *ZDHHC15* as a good candidate for SMS-like manifestation and prompt us to further elucidate its molecular pathways in connection with *RAI1* and circadian rhythms throughout *in vitro* silencing experiments on BE(2)-M17 human neuroblastoma cells. Remarkably RT-qPCR data revealed a marked upregulation of *RAI1* transcripts in *ZDHHC15* silenced samples, while no differences in *ZDHHC15* expression was observed in *RAI1* silenced samples. This result, even if not significant, revealed that ZDHHC15 could have an effect on *RAI1* transcript regulation by an indirect connection due to its role in post-translational regulation. Indeed, in this hypothesis ZDHHC15 might palmitoylate RAI1 transcriptional regulators, thus leading to its overexpression.

According to *RAI1* overexpression identified in *ZDHHC15* knocked-down cells, it seems that this gene might be not related to SMS where *RAI1* haploinsufficiency is found. Intriguingly *RAI1*

overexpression is the molecular cause of Potocki-Lupski (PTLS, OMIM#610883), a syndrome that shares with SMS several traits but an overall milder phenotype and represents one of SMS differential diagnosis chance. Indeed both SMS1 and SMS2 patients present most of the clinical signs shared between SMS and PTLS (i.e. short stature, brachydactyly, cardiovascular abnormalities, hypotonia, speech delay, Developmental Delay, Intellectual Disability, sleep disturbance, seizures, hyperactivity, ASD).

Moreover RT-qPCR analyses showed an overall upregulation, even if not significant, of *RAI1* putative positive regulators *HDAC4* and *MBD5* in *ZDHHC15* silenced samples. These data allowed us to further postulate that ZDHHC15 might exert an indirect control on *RAI1* transcription. On the other hand, as previously reported (Williams et al 2010 b; Mullegama et al 2015 a), no change in *HDAC4* and *MBD5* expression was observed in *RAI1* silenced samples. Thus *HDAC4*, *MBD5* upregulation and *RAI1* overexpression in *ZDHHC15* silenced samples are consistent with a role for ZDHHC15 in RAI1 modulation and in line with previously reported data (Williams et al 2010 b; Mullegama et al 2015 a).

Among 14 circadian regulators transcripts levels tested in BE(2)-M17 *RAI1* silenced samples, 7 resulted significantly dysregulated, 5 unaffected and 2 showed a dysregulation trend. In particular, *PER3* and *CRY1* significant downregulation showed on BE(2)-M17 is consistent with the data observed in HEK293T *RAI1* silenced samples (Williams et al 2012). On the contrary *CLOCK*, *BMAL1* and *NR1D2* levels observed in BE(2)-M17 *RAI1* silenced samples are unaffected and *NR1D1* and *RORC* are upregulated showing an opposite trend compared to HEK293T (Williams et al 2012). Upregulation as well as no differences observed for some of the circadian genes might reflect a cell specificity trend. It is likely that a neuroblastoma, as CNS tissue derived cell line, may have a different homeostasis of main circadian genes.

Regarding *ZDHHC15* silenced BE(2)-M17 samples, 6 out of 14 circadian regulators transcripts levels resulted significantly deregulated, 4 did not change and 4 displayed a deregulated trend. Among significantly downregulated genes tested, *PER3* resulted consistent with a recent report on Potocki Lupski patient synchronized lymphoblasts (Mullegama et al 2017).

Strikingly both *RAI1* and *ZDHHC15* silenced cells displayed significant deregulation of expression in up to half of the circadian genes tested thus sustaining an interconnection among ZDHHC15, RAI1 and circadian rhythms. Specifically, *CLOCK* and *PER1* expression levels did not change,

PER3 resulted downregulated while *RORC* markedly upregulated, in both *RAI1* and *ZDHHC15* knockdown cells. Further analysis are needed to clarify how ZDHHC15, RAI1 and circadian rhythms are connected each other (mechanistic insight).

In conclusion the data discussed further corroborate the hypothesis of *ZDHHC15* as novel candidate gene possibly explaining SMS-like condition. Useful approaches to clarify the detailed connection between RAI1 and ZDHHC15 might be transcriptomic and/or proteomic studies on in vitro model BE(2)-M17 and patients derived iPS cells.

REFERENCES

Albrecht U. Circadian clocks and circadian rhythms. Neuron (2012) Apr 26;74(2):246-60.

Balsalobre A, Damiola F and Schibler U. A serum shock induces circadian gene expression in mammalian tissue culture cells. Cell (1998) 93: 929–937.

Baymaz HI, Fournier A, Laget S, Ji Z, Jansen PW et al. MBD5 and MBD6 interact with the human PR-DUB complex through their methyl-CpG-binding domain.Proteomics (2014) Oct;14(19):2179-89.

Bi W, Yan J, Stankiewicz P, Park SS, Walz K et al. Genes in a refined Smith-Magenis syndrome critical deletion interval on chromosome 17p11.2 and the syntenic region of the mouse. Genome Res. (2002) May;12(5):713-28.

Bi W, Ohyama T, Nakamura H, Yan J, Visvanathan J et al. Inactivation of Rai1 in mice recapitulates phenotypes observed in chromosome engineered mouse models for Smith-Magenis syndrome. Hum. Molec. Genet. (2005) 14: 983-995.

Bi W, Saifi GM, Girirajan S, Shi X, Szomju B et al. RAI1 point mutations, CAG repeat variation, and SNP analysis in non-deletion Smith-Magenis syndrome. Am. J. Med. Genet. (2006) 140A: 2454-2463.

Bi W, Saifi GM, Shaw CJ, Walz K, Fonseca P et al. Mutations of RAI1, a PHD-containing protein, in nondeletion patients with Smith-Magenis syndrome. Hum. Genet. (2004) 115: 515-524.

Böhm S, Frishman D, Mewes HW. Variations of the C2H2 zinc finger motif in the yeast genome and classification of yeast zinc finger proteins. Nucleic Acids Res. (1997) Jun 15;25(12):2464-9.

Boone PM, RJ Reiter, DG Glaze, DX Tan, JR Lupski and L Potocki. Abnormal circadian rhythm of melatonin in Smith Magenis syndrome patients with RAI1 point mutations. Am J Med Gen (2011) Aug; 15A (8):2024-7.

Boudreau EA, Johnson KP, Jackman AR, Blancato J, Huizing M et al. Review of disrupted sleep patterns in Smith-Magenis syndrome and normal melatonin secretion in a patient with an atypical interstitial 17p11.2 deletion. Am J Med Genet A (2009) Jul;149A(7):1382-91.

Brown A, Phelan MC, Patil S, Crawford E, Rogers RC, Schwartz C. Two patients with duplication of 17p11.2: the reciprocal of the Smith-Magenis syndrome deletion? Am. J. Med. Genet. (1996) 63: 373-377.

Campbell IM Yuan B, Robberecht C, Pfundt R, Szafranski P, McEntagart ME et al. Parental somatic mosaicism is underrecognized and influences recurrence risk of genomic disorders. Am J Hum Genet.(2014) Aug 7;95(2):173-82.

Carmona-Mora P, Canales CP, Cao L, Perez IC, Srivastava AK et al. RAI1 transcription factor activity is impaired in mutants associated with Smith-Magenis Syndrome. PLoS One (2012) 7(9):e45155.

Ceballos-Chavez M, Rivero S, Garcia-Gutierrez P et al. Control of neuronal differentiation by sumoylation of BRAF35, a subunit of the LSD1–CoREST histone demethylase complex. Proc. Natl Acad. Sci. USA (2012) 109(21), 8085–8090.

Chen KS, Manian P, Koeuth T, Potocki L, Zhao Q et al. Homologous recombination of a flanking repeat gene cluster is a mechanism for a common contiguous gene deletion syndrome. Nature Genet. (1997) 17: 154-163.

Chen L, Tao Y, Song F, Yuan X, Wang J et al. Evidence for genetic regulation of mRNA expression of the dosage-sensitive gene retinoic acid induced-1 (RAI1) in human brain. Sci Rep. (2016) 6:19010.

Darvekar S, C Rekdal, T Johansen and E Sjottem. A phylogenetic study of SPBP and RAI1: evolutionary conservation of chromatin binding modules. PLoS One (2013) Oct 18;8(10):e78907.

De Leersnyder H, de Blois MC, Claustrat B, Romana S, Albrecht U et al. Inversion of the circadian rhythm of melatonin in the Smith-Magenis syndrome. J. Pediat. (2001) 139: 111-116.

De Leersnyder H, de Blois MC, Vekemans M, Sidi D, Villain E et al. Beta-1-adrenergic antagonists improve sleep and behavioural disturbances in a circadian disorder, Smith-Magenis syndrome. J. Med. Genet.(2003) 38: 586-590.

Dykens EM, Smith AC. Distinctiveness and correlates of maladaptive behaviour in children and adolescents with Smith-Magenis syndrome. J Intellect Disabil Res. (1998) Dec;42 (Pt 6):481-9.

Eberl HC, Spruijt CG, Kelstrup CD, Vermeulen M, Mann M. A map of general and specialized chromatin readers in mouse tissues generated by label-free interaction proteomics. Mol. Cell (2013) 49(2), 368–378.

Ebert DH, Greenberg ME. Activity-dependent neuronal signalling and autism spectrum disorder. Nature (2013) 493(7432), 327–337.

Edelman EA, Girirajan S, Finucane B, Patel PI, Lupski JR et al. Gender, genotype, and phenotype differences in Smith-Magenis syndrome: a meta-analysis of 105 cases. Clin. Genet. (2007) 71: 540-550.

el-Husseini Ael D and Bredt DS. Protein palmitoylation: a regulator of neuronal development and function, Nat Rev Neurosci (2002) 3, 791-802.

Elsea SH, Williams SR. Smith-Magenis syndrome: haploinsufficiency of RAI1 results in altered gene regulation in neurological and metabolic pathways. Expert Rev Mol Med. (2011) Apr 19;13:e14.

Elsea SH, Girirajan S. Smith-Magenis syndrome. Eur J Hum Genet. (2008) Apr;16(4):412-21.

Emery P, Reppert SM. A rhythmic Ror. Neuron (2004) 43, 443–446.

Fukata Y, M Fukata. Protein palmitoylation in neuronal development and synaptic plasticity. Nat Rev Neurosci (2010) Mar;11(3):161-75.

Gallego M, Virshup DM. Post-translational modifications regulate the ticking of the circadian clock. Nat. Rev. Mol. Cell Biol. (2007) 8, 139–148.

Garay PM, Wallner MA, Iwase S. Yin-yang actions of histone methylation regulatory complexes in the brain. Epigenomics (2016) Dec;8(12):1689-1708.

Giardino D, Finelli P, Gottardi G, De Canal G, Della Monica M et al. Narrowing the candidate region of Albright hereditary osteodystrophy-like syndrome by deletion mapping in a patient with an unbalanced cryptic translocation t(2;6)(q37.3;q26). Am. J. Med. Genet. (2003) 122A: 261-265.

Girirajan S, Patel N, Slager RE, Tokarz ME, Bucan M et al. How much is too much? Phenotypic consequences of Rai1 overexpression in mice. Eur J Hum Genet. (2008) Aug;16(8):941-54.

Girirajan S, Elseas LJII, Devriendt K, Elsea SH. RAI1 variations in Smith-Magenis syndrome patients without 17p11.2 deletions. J. Med. Genet. (2005) 42: 820-828.

Girirajan S, Truong HT, Blanchard CL, Elsea SH. A functional network module for Smith-Magenis syndrome. Clin Genet. (2009) 75(4):364–374.

Greco D, Romano C, Reitano S, Barone C, Benedetto DD et al. Three new patients with dup(17)(p11.2p11.2) without autism. Clin. Genet. (2008) 73: 294-296.

Greenberg F, Guzzetta V, Montes de Oca-Luna R, Magenis RE, Smith ACM et al. Molecular analysis of the Smith-Magenis syndrome: a possible contiguous-gene syndrome associated with del(17)(p11.2). Am. J. Hum. Genet. (1991) 49: 1207-1218.

Greenberg F, Lewis RA, Potocki L, Glaze D, Parke J et al. Multi-disciplinary clinical study of Smith-Magenis syndrome (deletion 17p11.2). Am. J. Med. Genet. (1996) 62: 247-254.

Gropman AL, Duncan WC, Smith AC. Neurologic and developmental features of the Smith-Magenis syndrome (del 17p11.2). Pediatr Neurol. (2006) May;34(5):337-50.

Huang WH, Guenthner CJ, Xu J, Nguyen T, Schwarz LA et al. Molecular and Neural Functions of Rai1, the Causal Gene for Smith-Magenis Syndrome. Neuron (2016) Oct 19;92(2):392-406.

Jean-Marcais N, Decamp M, Gerard M, Ribault V, Andrieux J et al. The first familial case of inherited 2q37.3 interstitial deletion with isolated skeletal abnormalities including brachydactyly type E and short stature. Am. J. Med. Genet. (2015) 167A: 185-189.

John B, Enright AJ, Aravin A, Tuschl T, Sander C, Marks DS. Human MicroRNA targets. PLoS Biol. (2005) Jul;3(7):e264.

Jones WD, Dafou D, McEntagart M et al. De novo mutations in MLL cause Wiedemann–Steiner syndrome. Am. J. Hum. Genet. (2012) 91(2), 358–364.

Kiriakidou M, Nelson PT, Kouranov A, Fitziev P, Bouyioukos C et al. A combined computational-experimental approach predicts human microRNA targets. Genes Dev. (2004) May 15;18(10):1165-78

Lacaria M, Gu W, Lupski JR. Circadian abnormalities in mouse models of Smith-Magenis syndrome: evidence for involvement of RAI1. Am J Med Genet A. (2013) Jul;161A(7):1561-8.

Laget SM, Joulie F Le Masson, N Sasai, E Christians, S Prandhan et al. The human proteins MBD5 and MBD6 associate with heterochromatin but they do not bind methylated DNA. Plos one (2010) (10) Aug: e11982.

Lewis BP, Burge CB, Bartel DP. Conserved Seed Pairing, Often Flanked by Adenosines, Indicates that Thousands of Human Genes are MicroRNA Targets. Cell (2005) 120:15-20.

Linder ME and Deschenes RJ. New insights into the mechanisms of protein palmitoylation, Biochemistry (2003) 42, 4311-4320

Liu P, Lacaria M, Zhang F, Withers M, Hastings PJ, Lupski JR. Frequency of nonallelic homologous recombination is correlated with length of homology: evidence that ectopic synapsis precedes ectopic crossing-over. Am. J. Hum. Genet. (2011) 89: 580-588.

Lobo S, Greentree WK, Linder ME, Deschenes RJ. Identification of a Ras palmitoyltransferase in Saccharomyces cerevisiae. J Biol Chem. (2002) Oct 25;277(43):41268-73.

Loebrich S, Nedivi E. The function of activity-regulated genes in the nervous system. Physiol. Rev. (2009) 89(4), 1079-1103.

Lowrey PL & Takahashi JS. Genetics of circadian rhythms in mammalian model organisms. Adv. Genet (2011) 74, 175-230.

Lowrey PL & Takahashi JS. Mammalian circadian biology: elucidating genome-wide levels of temporal organization. Annu. Rev. Genomics Hum. Genet. (2004) 5, 407-441.

Lupiáñez DG, Kraft K, Heinrich V, Krawitz P, Brancati F et al. Disruptions of topological chromatin domains cause pathogenic rewiring of gene-enhancer interactions. Cell. (2015) May 21;161(5):1012-1025.

Lupiáñez DG, Spielmann M, Mundlos S. Breaking TADs: How Alterations of Chromatin Domains Result in Disease. Trends Genet. (2016) Apr;32(4):225-37.

Lupski JR, Stankiewicz P. Genomic disorders: molecular mechanisms for rearrangements and conveyed phenotypes. PLoS Genet. (2005) Dec;1(6):e49.

Mansouri MR, L Marklund, P Gustavsson, E Davey, B Carlsson et al. Loss of ZDHHC15 expression in a woman with a balanced translocation t(X;15)(q13.3;cen) and severe mental retardation. Eur J Hum Genet. (2005) 13(8): p. 970-7.

Mitchell DA, Mitchell G, Ling Y, Budde C, Deschenes RJ. Mutational analysis of Saccharomyces cerevisiae Erf2 reveals a two-step reaction mechanism for protein palmitoylation by DHHC enzymes. J Biol Chem. (2010) Dec 3;285(49):38104-14.

Mitchell DA, A Vasudevan, ME Linder and RJ Deschenes. Protein palmitoylation by a family of DHHC protein S-acyltransferases. J Lipid Res (2006) Jun;47(6):1118-27.

Moncla A, Livet MO, Auger M, Mattei JF, Mattei MG, Giraud F. Smith-Magenis syndrome: a new contiguous gene syndrome: report of three new cases. J. Med. Genet. (1991) 28: 627-632.

Mullegama SV, Alaimo JT, Fountain MD, Burns B, Balog AH et al. RAI1 Overexpression Promotes Altered Circadian Gene Expression and Dyssomnia in Potocki-Lupski Syndrome. J Pediatr Genet. (2017) Sep;6(3):155-164.

Mullegama SV, L Pugliesi, B Burns, Z Shah, R Tahir et al. MBD5 haploinsufficiency is associated with sleep disturbance and disrupts circadian pathways common to Smith Magenis and Fragile X syndromes. Eur J Hum Gen (2015) 23(6): 781-9. (b)

Mullegama SV, Alaimo JT, Chen L, Elsea SH. Phenotypic and molecular convergence of 2q23.1 deletion syndrome with other neurodevelopmental syndromes associated with autism spectrum disorder. Int. J. Molec. Sci. (2015) 16: 7627-7643. (a)

Neira-Fresneda J, Potocki L. Neurodevelopmental Disorders Associated with Abnormal Gene Dosage: Smith-Magenis and Potocki-Lupski Syndromes. J Pediatr Genet. (2015) Sep;4(3):159-67.

Ohno Y, Kihara A, Sano T, Igarashi Y. Intracellular localization and tissue-specific distribution of human and yeast DHHC cysteine-rich domain-containing proteins. Biochim Biophys Acta (2006) Apr;1761(4):474-83.

Patil SR, Bartley JA. Interstitial deletion of the short arm of chromosome 17. Hum. Genet. (1984) 67: 237-238.

Potocki L, Bi W, Treadwell-Deering D, Carvalho CMB, Eifert A et al. Characterization of Potocki-Lupski syndrome (dup(17)(p11.2p11.2)) and delineation of a dosage-sensitive critical interval that can convey an autism phenotype. Am. J. Hum. Genet. (2007) 80: 633-649.

Potocki L, Chen KS, Park SS, Osterholm DE, Withers MA et al. Molecular mechanism for duplication 17p11.2 the homologous recombination reciprocal of the Smith-Magenis microdeletion. Nature Genet. (2000) 24: 84-87.

Potocki L, Glaze D, Tan DX, Park SS, Kashork CD, Shaffer LG, Reiter RJ, Lupski JR. Circadian rhythm abnormalities of melatonin in Smith-Magenis syndrome. J. Med. Genet. (2000) 37: 428-433.

Preussner M & Heyd F. Post-transcriptional control of the mammalian circadian clock: implications for health and disease. Pflugers Arch. (2016) 468, 983–991.

Rehmsmeier, Marc and Steffen, Peter and Hoechsmann, Matthias and Giegerich R. Fast and effective prediction of microRNA/target duplexes RNA, RNA (2004).

Ricard G, Molina J, Chrast J, Gu W, Gheldof N et al. Phenotypic consequences of copy number variation: insights from Smith-Magenis and Potocki-Lupski syndrome mouse models. PLoS Biol. (2010) Nov 23;8(11):e1000543.

Ripperger JA, Schibler U. Rhythmic CLOCK–BMAL1 binding to multiple E-box motifs drives circadian Dbp transcription and chromatin transitions. Nat. Genet. (2006) 38(3), 369-374.

Sanders SS, Martin DD, Butland SL, Lavallée-Adam M, Calzolari D et al. Curation of the Mammalian Palmitoylome Indicates a Pivotal Role for Palmitoylation in Diseases and Disorders of the Nervous System and Cancers. PLoS Comput Biol. (2015) Aug 14;11(8):e1004405.

Sando R, N Gounko, S Pieraut, L Liao, J Yates III and Anton Maximov. HDAC4 governs a transcriptional program essential for Synaptic Plasticity and memory. Cell. (2012) Nov 151:821-834.

Sarimski K. Communicative competence and behavioural phenotype in children with Smith-Magenis syndrome. Genet Couns. (2004) 15(3):347-55.

Shaw CJ, Lupski JR. Non-recurrent 17p11.2 deletions are generated by homologous and non-homologous mechanisms. Hum Genet. (2005) Jan;116(1-2):1-7.

Shaw CJ, Bi W, Lupski JR. Genetic proof of unequal meiotic crossovers in reciprocal deletion and duplication of 17p11.2. Am. J. Hum. Genet. (2002) 71: 1072-1081.

Shaw CJ, Withers MA, Lupski J. R. Uncommon deletions of the Smith-Magenis syndrome region can be recurrent when alternate low-copy repeats act as homologous recombination substrates. Am. J. Hum. Genet. (2004) 75: 75-81.

Slager RE, Newton TL, Vlangos CN, Finucane B, Elsea SH. Mutations in RAI1 associated with Smith-Magenis syndrome. Nature Genet. (2003) 33: 466-468.

Smith AC, Dykens E, Greenberg F. Behavioral phenotype of Smith-Magenis syndrome (del 17p11.2).Am J Med Genet. (1998) Mar 28;81(2):179-85.

Smith AC, Dykens E, Greenberg F. Sleep disturbance in Smith-Magenis syndrome (del 17 p11.2). Am J Med Genet. (1998) Mar 28;81(2):186-91.

Smith ACM, Gropman AL, Bailey-Wilson JE, Goker-Alpan O, Elsea SH et al. Hypercholesterolemia in children with Smith-Magenis syndrome: del (17)(p11.2p11.2). Genet. Med. (2002) 4: 118-125.

Smith ACM, McGavran L, Robinson J, Waldstein G, Macfarlane J et al. Interstitial deletion of (17)(p11.2p11.2) in nine patients. Am. J. Med. Genet. (1986) 24: 393-414.

Stankiewicz P, Lupski JR. Genome architecture, rearrangements and genomic disorders. Trends Genet. (2002) 18: 74-82.

Tahir R, A Kennedy, SH Elsea and AJ Dickinson, Retinoic acid induced-1 (Rai1) regulates craniofacial and brain development in Xenopus. Mech Dev. (2014) Aug;133:91-104.

Takahashi JS. Transcriptional architecture of the mammalian circadian clock. Nat Rev Genet. (2017) Mar;18(3):164-179.

Talkowski ME, Mullegama SV, Rosenfeld JA, van Bon BW, Shen Y et al. Assessment of 2q23.1 microdeletion syndrome implicates MBD5 as a single causal locus of intellectual disability, epilepsy, and autism spectrum disorder. Am J Hum Genet. (2011) Oct 7;89(4):551-63.

Toulouse A, Rochefort D, Roussel J, Joober R, Rouleau GA. Molecular cloning and characterization of human RAI1, a gene associated with schizophrenia. Genomics (2003) 82(2), 162-171.

Truong HT, Dudding T, Blanchard CL, Elsea SH. Frameshift mutation hotspot identified in Smith-Magenis syndrome: case report and review of literature. BMC Med Genet. (2010) Oct 8;11:142.

Ueda HR, Chen W, Adachi A, Wakamatsu H, Hayashi S et al. A transcription factor response element for gene expression during circadian night. Nature. (2002); 418: 534-539.

Ueda HR, Hayashi S, Chen W, Sano M, Machida M et al. System-level identification of transcriptional circuits underlying mammalian circadian clocks. Nat. Genet. (2005); 37: 187-192.

van Bon BWM, Koolen DA, Brueton L, McMullan D, Lichtenbelt KD et al. The 2q23.1 microdeletion syndrome: clinical and behavioural phenotype. Europ. J. Hum. Genet. (2010) 18: 163-170.

Van Der Zwaag B, Franke L, Poot M et al. Gene-network analysis identifies susceptibility genes related to glycobiology in autism. PLoS ONE (2009) 4(5).

Vieira GH, Rodriguez JD, Carmona-Mora P, Cao L, Gamba BF et al. Detection of classical 17p11.2 deletions, an atypical deletion and RAI1 alterations in patients with features suggestive of Smith-Magenis syndrome. Eur J Hum Genet. (2012) Feb;20(2):148-54.

Vilboux T, Ciccone C, Blancato JK, Cox GF, Deshpande C et al. Molecular analysis of the retinoic acid induced 1 gene (RAI1) in patients with suspected Smith-Magenis syndrome without the 17p11.2 deletion. PLoS One (2011) 6: e22861.

Villavicencio-Lorini P, Klopocki E, Trimborn M, Koll R, Mundlos S, Horn D. Phenotypic variant of brachydactyly-mental retardation syndrome in a family with an inherited interstitial 2q37.3 microdeletion including HDAC4. Europ. J. Hum. Genet. (2013) 21: 743-748.

Wagenstaller J, Spranger S, Lorenz-Depiereux B, Kazmierczak B, Nathrath M et al. Copy-number variations measured by single-nucleotide-polymorphism oligonucleotide arrays in patients with mental retardation. Am. J. Hum. Genet. (2007) 81: 768-779.

Walz K, Caratini-Rivera S, Bi W, Fonseca P, Mansouri DL et al. Modeling del(17)(p11.2p11.2) and dup(17)(p11.2p11.2) contiguous gene syndromes by chromosome engineering in mice: phenotypic consequences of gene dosage imbalance. Molec. Cell. Biol. (2003) 23: 3646-3655.

Walz K, Paylor R, Yan J, Bi W, Lupski JR. Rai1 duplication causes physical and behavioral phenotypes in a mouse model of dup(17)(p11.2 p11.2). J. Clin. Invest. (2006) 116: 3035-3041.

Walz K, Spencer C, Kaasik K, Lee CC, Lupski JR, Paylor R. Behavioral characterization of mouse models for Smith-Magenis syndrome and dup(17)(p11.2p11.2). Hum. Molec. Genet. (2004) 13: 367-378.

Wang F, Chen X, Shi W, Yao L, Gao M, Yang Y, Hao A. Zdhhc15b Regulates Differentiation of Diencephalic Dopaminergic Neurons in zebrafish. J Cell Biochem. (2015) Dec; 116(12):2980-91.

Wheeler PG, Huang D, Dai Z. Haploinsufficiency of HDAC4 does not cause intellectual disability in all affected individuals. Am. J. Med. Genet. (2014) 164A: 1826-1829.

Williams SR, Aldred MA, Der Kaloustian VM, Halal F, Gowans G et al. Haploinsufficiency of HDAC4 causes brachydactyly mental retardation syndrome, with brachydactyly type E, developmental delays, and behavioral problems. Am J Hum Genet. (2010) Aug 13;87(2):219-28. (b)

Williams SR, Girirajan S, Tegay D, Nowak N, Hatchwell E, Elsea SH. Array comparative genomic hybridisation of 52 subjects with a Smith-Magenis-like phenotype: identification of dosage sensitive loci also associated with schizophrenia, autism, and developmental delay. J Med Genet. (2010) Apr;47(4):223-9. (a)

Williams SR, Mullegama SV, Rosenfeld JA, Dagli AI, Hatchwell E et al. Haploinsufficiency of MBD5 associated with a syndrome involving microcephaly, intellectual disabilities, severe speech impairment and seisure. Eur J Hum Genet (2010) 18: 436-441. (c)

Williams SR, Zies D, Mullegama SV, Grotewiel MS, Elsea SH. Smith-Magenis syndrome results in disruption of CLOCK gene transcription and reveals an integral role for RAI1 in the maintenance of circadian rhythmicity. Am. J. Hum. Genet. (2012) 90: 941-949.

Wilson LC, Leverton K, Oude Luttikhuis MEM, Oley CA, Flint J et al. Brachydactyly and mental retardation: an Albright hereditary osteodystrophy-like syndrome localized to 2q37. Am. J. Hum. Genet. (1995) 56: 400-407.

Xiaowei Wang and Issam M El Naqa. Prediction of both conserved and nonconserved microRNA targets in animals. Bioinformatics (2008) 24(3):325-332.

Young FB, SL Butland, SS Sanders, LM Sutton and MR Hayden Putting proteins in their place: palmitoylation in Huntington disease and other neuropsychiatric diseases. Prog Neurobiol. (2012) May;97(2):220-38.

Zhang F, Potocki L, Sampson JB, Liu P, Sanchez-Valle A et al. Identification of uncommon recurrent Potocki-Lupski syndrome-associated duplications and the distribution of rearrangement types and mechanisms in PTLS. Am. J. Hum. Genet. (2010) 86: 462-470.

Zhou F, Xue Y, Yao X, Xu Y. CSS-Palm: palmitoylation site prediction with a clustering and scoring strategy (CSS) Bioinformatics (2006) Apr 1;22(7):894-6.

Zori RT, Lupski JR, Heju Z, Greenberg F, Killian JM et al. Clinical, cytogenetic, and molecular evidence for an infant with Smith-Magenis syndrome born from a mother having a mosaic 17p11.2p12 deletion. Am. J. Med. Genet. (1993) 47: 504-511.

Acknowledgements

I would thank Prof Palma Finelli and Prof Antonia Ratti for mentoring and critical discussion related and not related to PhD project. Dr PhD Claudia Colombrita and Prof Silani lab members (Patrizia, Cinzia, Annamaria, Francesca, Valentina and Clara) for collaboration and scientific support. Regarding my lab collegues I'll be grateful to Dr PhD Ilaria Bestetti, Dr Alessandra Sironi and Dr Milena Crippa for everyday motivating and critical discussions and supportive/collaborative interaction.

Out of professional environment I wish to thank my parents and my closest friends Valentina and Daniela for sympathetic involvement in my goals.